# The Influence of Black Holes on Light Ray Trajectories

Conrad Brown

April 26, 2011

## Declaration of Authorship

This piece of work is a result of my own work except where it forms an assessment based on group project work. In the case of a group project, the work has been prepared in collaboration with other members of the group. Material from the work of others not involved in the project has been acknowledged and quotations and paraphrases suitably indicated.

## Abstract

A discussion of light trajectories in Schwarzschild and Kerr geometry with particular emphasis placed on black holes. These fall into three categories; Plunge, Scatter and unstable circular trajectories. The type of trajectory depends on the impact parameter ($b$) of the light ray, the mass ($M$) and the angular momentum ($J$) of the black hole. Only trajectories external to the event horizon, and starting a large distance from the black hole are considered.

## Acknowledgments

Firstly I would like to thank my supervisors Prof. Ruth Gregory and Prof. Simon Ross for their invaluable advice and guidance with both the subject matter and the technicalities in producing an academic report. I would also like to thank Mr Chris Brown for being my test third year maths student. Finally I would like to thank my family for offering proofreading help.

# Contents

# List of Figures

# 1 Introduction

In Newtonian mechanics light is not affected by the influence of gravity moving only in straight lines[1]. One of the most interesting, and most readily testable, facets of Einstein's General Relativity theory is that massive objects cause light trajectories to curve. This report explores this phenomenon with particular attention applied to the most extreme case: black holes.

In the first two sections we set ourselves up with the mathematical tools required to study non-Euclidean geometries, and review some important aspect of special relativity and their generalizations. We go on to look, in Section 4, at the simplest, relevant non-Euclidean geometry which is that surrounding non-rotating, changeless, spherically symmetric masses. This geometry is named after Karl Schwarzschild (1873-1916)[2] who devised the first set of solutions to the Einstein field equations while serving on the eastern front during the First World War. These solutions describe the geometry that is his namesake.

In Section 4.5 we study the different types of trajectory that light can take in Schwarzschild geometry. We note that these fall into three qualitatively distinct categories; plunge, scatter and circular orbits. We examine some properties of these orbits before going on to discuss, in Section 5, gravitational lensing as a consequence of scatter orbits. We use this phenomena to produce an approximate equation that relates the mass of the lens to various measurable distances and angles.

Finally we look at rotating black holes[3], called Kerr black holes, which are named after Roy Kerr (1934-present)[4]. In order to maintain as much symmetry as we can, in the Kerr case, we focus on equatorial orbits where the classification system we applied to light trajectories in Schwarzschild geometry still applies and is still exhaustive for orbits from infinity.

## 1.1 A Note on Notation

Throughout this document we use notations and conventions broadly the same as those found in Hartle [1], as he forms the primary source for much of my preliminary work. Where Hartle does not form part of the source material I have altered notation to be in line with his where a precedent has already been set in the document, and adopted the notation of other authors in the few occasions when no such precedent existed.

[1] This is in its traditional formulation. There are formulations in which light curves, normally by assigning mass to light 'corpuscles'. The curvature produced in general relativity is greater than in these Newtonian formulations and does not require the non-physical assumption of massive light.

[2] See Weisstein [13].

[3] An interesting consequence of complete gravitational collapse is that much of the information about the state of matter is lost, leaving only three attributes which completely determine the properties of the black hole. These are mass, charge and angular momentum. See Bekenstein [10].

[4] See the Encyclopaedia Britannica's website [14].

# 2 Non-Euclidean Geometries

## 2.1 The Metric and Line Element

In General Relativity spacetime is curved by massive objects. To understand curved spaces we need a non-Euclidean geometry. Such a geometry will have some structure to it and we will need some way to describe how this structure changes, with respect to spatial translations. We use the line element to do this as it gives us function of how the space changes locally. Thus to find global changes we integrate across the relevant domain. It is clear that this requires us to deal with differentiable spaces and for this reason we do not discuss what happens at singularities. In this Section we discuss material similar to that found in Hartle [1] - Section 7.2.

A geometry in coordinates $x^\alpha$ is described by the line element:

$$ds^2 = g_{\alpha\beta}(x)\, dx^\alpha dx^\beta \tag{1}$$

where $g_{\alpha\beta}(x)$ is a symmetric, position dependent, matrix called the metric[5]. As we are dealing with four-dimensional spaces, with coordinates $x^\alpha = (x^0, x^1, x^2, x^3)$, the general form is:

$$g_{\alpha\beta}(x) = \begin{bmatrix} g_{00}(x^\alpha) & g_{01}(x^\alpha) & g_{02}(x^\alpha) & g_{03}(x^\alpha) \\ g_{01}(x^\alpha) & g_{11}(x^\alpha) & g_{12}(x^\alpha) & g_{13}(x^\alpha) \\ g_{02}(x^\alpha) & g_{12}(x^\alpha) & g_{22}(x^\alpha) & g_{23}(x^\alpha) \\ g_{03}(x^\alpha) & g_{13}(x^\alpha) & g_{23}(x^\alpha) & g_{33}(x^\alpha) \end{bmatrix}.$$

For example the metric for four-dimensional Euclidean space, in Cartesian coordinates $x^\alpha = (w, x, y, z)$, is:

$$\begin{bmatrix} 1 & 0 & 0 & 0 \\ 0 & 1 & 0 & 0 \\ 0 & 0 & 1 & 0 \\ 0 & 0 & 0 & 1 \end{bmatrix}. \tag{2}$$

The metric for the flat (Minkowski) spacetime ($\eta_{\alpha\beta}$) of inertial frames, in Cartesian coordinates $x^\alpha = (t, x, y, z)$, is:

$$\eta_{\alpha\beta} = \begin{bmatrix} -1 & 0 & 0 & 0 \\ 0 & 1 & 0 & 0 \\ 0 & 0 & 1 & 0 \\ 0 & 0 & 0 & 1 \end{bmatrix}. \tag{3}$$

We will meet some other metrics that represent curved spacetimes later.

The distance $\Delta s$ between two points $a$ and $b$ in the geometry is given by

$$\Delta s = \int_a^b ds \tag{4}$$

[5] Here and elsewhere we make use of the Einstein summation convention.

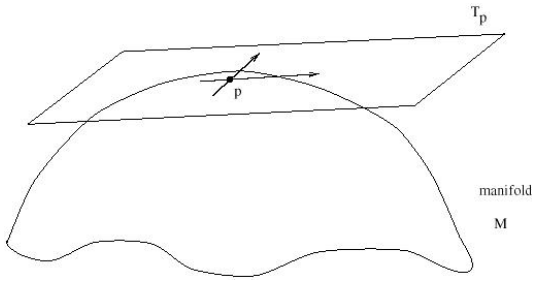


Figure 1: Here we have a two-dimensional manifold sat in three-dimensional Euclidean space. The tangent space $T_p$ to the manifold $\mathfrak{M}$ at $P$ is indicated and is the set of all vectors tangential to any curve $\gamma \in \mathfrak{M}$ at $P$. We can increase the number of dimensions as required.
Source: Carroll (1997) [15]

## 2.2 Scalar Products in Non-Euclidean Geometries

To perform calculations in non-Euclidean geometries we need some notion of a scalar product. To do this we consider the geometry to be that of the surface of a manifold in some higher dimensional Euclidean space. It is possible to do this more generally, without the need for embedding in Euclidean space, however the result is the same and this discussion is more intuitive. The information in this Section was sourced from Hobson et al. [3] - Chapter 3. For a more detailed discussion of manifolds see O'Neill [6] - Chapter 1.

The tangent space $T_p$ to a manifold $\mathfrak{M}$ at any point $P$ is the set of all vectors tangential to any curve $\gamma \in \mathfrak{M}$ at $P$. So any local vector $v$ in $\mathfrak{M}$ at $P$ lies in $T_p$ and $T_p$ is the set of such vectors. This is illustrated in Figure 1 as a two-dimensional manifold sat in three-dimensional Euclidean space. We can expand to greater dimensions as required.

The tangent plane is independent of the coordinate system used to define points on the manifold, however we may define at each point $P$ a set of basis vectors $\mathbf{e}_\alpha$ for $T_p$ allowing us to express any vector $\mathbf{v}$ at $P$ as a linear combination of these basis vectors. This allows us to express the local vector field $\mathbf{v}(x)$, at each point, in terms of the basis vectors like so:

$$\mathbf{v}(x) = v^\alpha(x)\mathbf{e}_\alpha(x). \tag{5}$$

If we choose our local tangent space basis vectors $\mathbf{e}_\alpha$ to be tangential to our manifold coordinates $x^\alpha$ (whatever choice we have already made for $x^\alpha$) these are called the coordinate basis, and are defined as:

$$\mathbf{e}_\alpha = \lim_{\delta x^\alpha \to 0} \frac{\delta \mathbf{s}}{\delta x^\alpha} \tag{6}$$

where $\delta\mathbf{s}$ is an infinitesimal displacement vector between the point $P$ and a

point in the neighborhood of $P$ that is a distance $\delta x^\alpha$ along the coordinate curve $x^\alpha$. The set $e_\alpha$ are linearly independent since the $x^\alpha$ are. There are the same number of $e_\alpha$ as there are $x^\alpha$ and therefore there are the same number of $e_\alpha$ as dimension of the tangent space. From this we conclude that $e_\alpha$ forms a basis of the tangent space. We can now see from equation (6) that:

$$d\mathbf{s} = \mathbf{e}_\alpha(x)dx^\alpha. \tag{7}$$

Using equation (7), in combination with equation (1), we get:

$$g_{\alpha\beta}(x)\,dx^\alpha dx^\beta = ds^2 = d\mathbf{s}\cdot d\mathbf{s} = \mathbf{e}_\alpha(x)\,dx^\alpha \cdot \mathbf{e}_\beta(x)\,dx^\beta = (\mathbf{e}_\alpha(x)\cdot\mathbf{e}_\beta(x))\,dx^\alpha dx^\beta$$

$$\Rightarrow \mathbf{e}_\alpha(x)\cdot\mathbf{e}_\beta(x) = g_{\alpha\beta}(x). \tag{8}$$

Thus we have:

$$\mathbf{a}\cdot\mathbf{b} = g_{\alpha\beta}a^\alpha b^\beta \tag{9}$$

# 3 Special Relativity Extended

This Section discusses a few properties of Special Relativity that are relevant to our line of reasoning. It then extends these to the general case.

## 3.1 Units

It is to be remembered that, as in Special Relativity, we simplify our calculations by measuring time in metres and setting the speed of light $c = 1$ via the transformation $t(\text{in m}) = ct(\text{in s})$. In General Relativity we also measure mass in metres and set the gravitational constant $G = 1$ via the transformation $M(\text{in m}) = MG/c^2(\text{in kg})$. This system is called geometrized units and, unless otherwise stated, we make use of it. For a more detailed account of this see Hartle [1] - Section 4.6.

## 3.2 World Lines

The world line of an object is the path it takes through spacetime. This Section introduces a classification system of different types of world lines, basing the discussion on Hartle [1] - Section 4.3.

A property of a world line that we are interested in is the spacetime distance along it, which we can calculate using equation (4).

It is worth noting that the flat spacetime metric $\eta_{\alpha\beta}$ - see equation (3) - is not the same as the Euclidean metric (2). This difference means that in general $ds^2 \not> 0$. In particular it allows us to draw the distinction between timelike, lightlike and spacelike separated points in spacetime. As summarized below:

$$(\Delta s)^2 > 0 \Rightarrow \text{ spacelike}$$

$$(\Delta s)^2 = 0 \Rightarrow \text{ lightlike}$$
$$(\Delta s)^2 < 0 \Rightarrow \text{ timelike.} \tag{10}$$

This classification system still applies in general relativity.

## 3.3 Geodesics

### 3.3.1 Timelike Geodesics

It is known that in special relativity the variation principle, defined below, summarizes the equations of motion for objects uninfluenced by any force. Now we assume that this principle holds in the general case, and use it to construct equations of motion in curved spacetimes. Though we are concerning ourselves with the trajectories of light it is helpful to look first at the timelike geodesics of massive particles, using information sourced from Hartle [1] - Section 8.1. In the following section we look at the lightlike case which is based on Section 8.3 of the same.

Variational principle: the world line of a free test particle between two timelike separated points extremizes the proper time between them.

We assume throughout the discussion that the curvature of spacetime caused by these particles is negligible, and it is for this reason that we refer to test particles rather than particles. The Extrema of a function of n variables is where all the partial derivatives vanish. The particle being free means that the only thing influencing its trajectory is the curvature of spacetime and its initial conditions, this is distinct from how we use the term free in special relativity. In special relativity the variational principle holds when all forces, including gravity, are absent. However in general relativity gravity is not a force, but the result of spacetime curvature induced by the presence of mass. For this reason gravity's influence is not excluded for free particles in general relativity.

From equation (1), and the definition of proper time $d\tau^2 \equiv -ds^2$, we calculate the proper time interval along the world line of a timelike test particle moving from a point $A$ to a point $B$ via:

$$\tau_{AB} = \int_A^B d\tau = \int_A^B \left(-g_{\alpha\beta}\left(x\right) dx^\alpha dx^\beta\right)^{1/2}. \tag{11}$$

If we now parametrize $x^\alpha$ by a parameter $\sigma$, such that $\sigma = 0$ at $A$ and $\sigma = 1$ at $B$, we get:

$$\tau_{AB} = \int_0^1 d\sigma \left(-g_{\alpha\beta}\left(x\right) \frac{dx^\alpha}{d\sigma} \frac{dx^\beta}{d\sigma}\right)^{1/2} \tag{12}$$

A world line adheres to the variation principle if and only if it satisfy Lagrange's equation:

$$-\frac{d}{d\sigma}\left(\frac{\partial L}{\partial\left(\frac{dx^{\alpha}}{d\sigma}\right)}\right)+\frac{\partial L}{\partial x^{\alpha}}=0. \tag{13}$$

For the Lagrangian:

$$L=\left(g_{\alpha\beta}\left(x\right)\frac{dx^{\alpha}}{d\sigma}\frac{dx^{\beta}}{d\sigma}\right)^{1/2}. \tag{14}$$

Plugging equation (14) into equation (13) we get[6]:

$$-\frac{d}{d\sigma}\left[\left(-g_{\gamma\delta}\frac{dx^{\gamma}}{d\sigma}\frac{dx^{\delta}}{d\sigma}\right)^{-1/2}\left(g_{\alpha\beta}\frac{dx^{\beta}}{d\sigma}\right)\right]+\frac{1}{2}\left(-g_{\gamma\delta}\frac{dx^{\gamma}}{d\sigma}\frac{dx^{\delta}}{d\sigma}\right)^{-1/2}\frac{\partial g_{\varepsilon\beta}}{\partial x^{\alpha}}\frac{dx^{\varepsilon}}{d\sigma}\frac{dx^{\beta}}{d\sigma}=0. \tag{15}$$

We can now use equation (12) to get:

$$\frac{d\tau}{d\sigma}=\left(-g_{\alpha\beta}\left(x\right)\frac{dx^{\alpha}}{d\sigma}\frac{dx^{\beta}}{d\sigma}\right)^{1/2}. \tag{16}$$

Plugging this into equation (15) multiplied by $d\sigma/d\tau$ we find that:

$$-\frac{d}{d\tau}\left[g_{\alpha\beta}\left(x\right)\frac{dx^{\beta}}{d\tau}\right]+\frac{1}{2}\frac{\partial g_{\beta\gamma}}{\partial x^{\alpha}}\frac{dx^{\beta}}{d\tau}\frac{dx^{\gamma}}{d\tau}=0$$

$$\Rightarrow -g_{\alpha\beta}\frac{d^{2}x^{\beta}}{d\tau}-\frac{dg_{\alpha\beta}}{d\tau}\frac{dx^{\beta}}{d\tau}+\frac{1}{2}\frac{\partial g_{\beta\gamma}}{\partial x^{\alpha}}\frac{dx^{\beta}}{d\tau}\frac{dx^{\gamma}}{d\tau}=0$$

which, by the chain rule, implies:

$$-g_{\alpha\beta}\frac{d^{2}x^{\beta}}{d\tau^{2}}+\left(-\frac{\partial g_{\alpha\beta}}{\partial x^{\gamma}}+\frac{1}{2}\frac{\partial g_{\beta\gamma}}{\partial x^{\alpha}}\right)\frac{dx^{\beta}}{d\tau}\frac{dx^{\gamma}}{d\tau}=0$$

$$\Rightarrow g_{\alpha\delta}\frac{d^{2}x^{\delta}}{d\tau^{2}}=-\frac{1}{2}\left(\frac{\partial g_{\alpha\beta}}{\partial x^{\gamma}}+\frac{\partial g_{\alpha\gamma}}{\partial x^{\beta}}-\frac{\partial g_{\beta\gamma}}{\partial x^{\alpha}}\right)\frac{dx^{\beta}}{d\tau}\frac{dx^{\gamma}}{d\tau}. \tag{17}$$

We now introduce the inverse metric $g^{\alpha\beta}$, so $g^{\alpha\beta}g_{\beta\gamma}=\delta_{\gamma}^{\alpha}$ where $\delta_{\gamma}^{\alpha}$ is the Kronecker delta. Multiplying equation (17) by $g^{\alpha\beta}$ we get:

$$\frac{d^{2}x^{\delta}}{d\tau^{2}}=-\frac{1}{2}g^{\delta\alpha}\left(\frac{\partial g_{\alpha\beta}}{\partial x^{\gamma}}+\frac{\partial g_{\alpha\gamma}}{\partial x^{\beta}}-\frac{\partial g_{\beta\gamma}}{\partial x^{\alpha}}\right)\frac{dx^{\beta}}{d\tau}\frac{dx^{\gamma}}{d\tau}. \tag{18}$$

We simplify this expression by introducing the Christoffel symbols $\Gamma_{\beta\gamma}^{\alpha}$which are calculated via

$$\Gamma_{\beta\gamma}^{\delta}\equiv\frac{1}{2}g^{\delta\alpha}\left(\frac{\partial g_{\alpha\beta}}{\partial x^{\gamma}}+\frac{\partial g_{\alpha\gamma}}{\partial x^{\beta}}-\frac{\partial g_{\beta\gamma}}{\partial x^{\alpha}}\right) \tag{19}$$

[6]At this point Hartle defers the rest of the derivation of the Geodesic equation (20) to an attachment on his website [16], which may be found in the web supplements Section and is entitled Chapter 8: Derivation of the General Geodesic Equation.

and thus equation (18) becomes

$$\frac{d^2x^\alpha}{d\tau^2} = -\Gamma^\alpha_{\beta\gamma}\frac{dx^\beta}{d\tau}\frac{dx^\gamma}{d\tau}. \tag{20}$$

Equation (20) is called the geodesic equation. A geodesic is a generalization of the notion of a straight line in flat spacetime. Equivalently a path between 2 points, in some geometry, is a geodesic if it is locally the shortest path between those points, in that geometry. A curve is a geodesic if and only if it adheres to the geodesic equation

We have shown that trajectories that adhere to the variation follow geodesics in a curved spacetime, there is a large amount of evidence that real world trajectories do adhere to the variation principle and indeed follow geodesics.

The geodesic equation consists of coupled, second order ODEs. As we are dealing with four-dimensional spacetime there are four of them. However it is worth noting that $\Gamma^\alpha_{\beta\gamma}$ is a rank three tensor and therefore has $4^3 = 64$ components. For this reason calculating its components is arduous and time consuming to perform explicitly so we will use Mathematica to perform the calculations for us.

### 3.3.2 Null Geodesics

The geodesic equation, as we have constructed it, restricts the motion of timelike particles however we are interested in the motion of light. We need a similar equation that tells us about the motion of lightlike objects which we will find in this Section. The information found herein was sourced from Hartle [1] - Section 8.3.

A null geodesic is similar to those discussed above however it is lightlike and so it describes the trajectories of photons (and other massless particles). However $\tau$ ceases to be a useful parameter since the proper time experienced by light is always zero. For this reason we use another parameter which we denote $\lambda$. However we cannot just use any parameter without it changing the form of the Geodesic equation (20), so to keep things simple we stipulate that $\lambda$ is an affine parameter. That the parameter is affine means that it belongs to the class of parameters that do not change the form of the geodesic equation[7]. Thus we have:

$$\frac{d^2x^\alpha}{d\lambda^2} = -\Gamma^\alpha_{\beta\gamma}\frac{dx^\beta}{d\lambda}\frac{dx^\gamma}{d\lambda}. \tag{21}$$

The actual derivation of equation (21) involves generalizing the laws of electromagnetism to operating in curved spacetimes, which is beyond the scope of this project. However there are two things we know that we can use to motivate the result. Firstly we know from special relativity and Newtonian mechanics that in flat spacetime the equation of the motion of light rays is:

[7] See Hartle [1] - Section 5.5.

$$\frac{d^2x^\alpha}{d\lambda^2} = 0.$$

This is the statement that light moves in a straight line with constant velocity. Therefore we know that the general case must reduce to this in a local inertial frame. We further know that the equation must be of the same form for all coordinate systems, because we have used an arbitrary coordinate system throughout. From our discussion in Section 3.3.1 it is clear that equation (20) satisfies this second property, since no specific coordinate system was introduced in that discussion either, and so by analogy does equation (21). The first property follows since plugging the metric for flat spacetime $\eta_{\alpha\beta}$ into equation (19) we get:

$$\Gamma^\delta_{\beta\gamma} = \frac{1}{2}\eta^{\delta\alpha}\left(\frac{\partial\eta_{\alpha\beta}}{\partial x^\gamma} + \frac{\partial\eta_{\alpha\gamma}}{\partial x^\beta} - \frac{\partial\eta_{\beta\gamma}}{\partial x^\alpha}\right) = 0$$

since all the partial derivatives vanish. This is not surprising since our derivation of the geodesic equation (20) was a process of generalizing unaccelerated motion to curved spaces.

Now if we let $x^\alpha(\lambda)$ be the path of a light ray parametrized by some affine parameter $\lambda$ and $u^\alpha \equiv dx^\alpha/d\lambda$ be its tangent vector. From equations (1), (9) and the lightlike case in (10) we get:

$$\mathbf{u}\cdot\mathbf{u} = g_{\alpha\beta}(x)\frac{dx^\alpha}{d\lambda}\frac{dx^\beta}{d\lambda} = 0. \tag{22}$$

Which, along with equation (21), gives us all the equations we need to calculate light trajectories in some geometry.

# 4 Schwarzschild Geometry

Schwarzschild geometry is the geometry of spacetime outside a spherically symmetric mass at rest. The Schwarzschild black hole is the simplest model of a black hole and it is where we assume that the gravitationally collapsing body and spacetime outside it are spherically symmetric. We will now find the metric that describes such a geometry.

## 4.1 Finding the Schwarzschild Metric

To begin with we wish to construct the line element $ds^2$ of Schwarzschild geometry and, by equation (1), find the components of the metric $g_{\alpha\beta}$. To do this I have synthesized information found in Hobson et al. [3] - Section 9.1 and Chow [2] - Section 4.1.

The symmetries in the construction of Schwarzschild geometry tell us two things, which are;

- The metric $g_{\alpha\beta}$ will be independent of the time coordinate t, since the only mass influencing the geometry is at rest.

- The metric $g_{\alpha\beta}$ can only depend on quantities that are invariant under rotation. This is the condition that $ds$ depends solely on rotationally invariant quantities and their derivatives, i.e $ds$ is isotropic.

Rotational invariants of spacelike Euclidean coordinates $\mathbf{x} = (x, y, z)$ can only depend on the scaler quantities:

$$\mathbf{x} \cdot \mathbf{x}, \quad \mathbf{dx} \cdot \mathbf{dx}, \quad \mathbf{dx} \cdot \mathbf{x}. \tag{23}$$

Which in polar coordinates are:

$$\mathbf{x} \cdot \mathbf{x} = r^2, \ \ \mathbf{dx} \cdot \mathbf{dx} = dr^2 + r^2(d\theta^2 + \sin^2\theta d\phi^2), \ \ \mathbf{dx} \cdot \mathbf{x} = rdr. \tag{24}$$

Now we construct $ds^2$ in the most general possible way such that every term:

- contains the product of precisely two derivatives;
- is independent of time;
- is isotropic.

This gives:

$$ds^2 = -F(r)dt^2 + G(r)dt(\mathbf{dx} \cdot \mathbf{x}) + H(r)(\mathbf{dx} \cdot \mathbf{x})^2 + I(r)\mathbf{dx} \cdot \mathbf{dx}$$

$$= -F(r)dt^2 + G(r)rdtdr + H(r)(rdr)^2 + I(r)(dr^2 + r^2(d\theta^2 + \sin^2\theta d\phi^2))$$

for $F$, $G$, $H$ and $I$ general functions of $r$. This allows us, without loss of generality, to transform $F$, $G$, $H$ and $I$ by any function of $r$ and thus we can equate terms and absorb factors of $r$ giving[8]:

$$-F(r)dt^2 + G(r)dtdr + H(r)(dr)^2 + I(r)(d\theta^2 + \sin^2\theta d\phi^2).$$

We can now define a new radial coordinate $r$ via $r^2 = I(r)$ yielding[9]:

$$-F(r)dt^2 + G(r)dtdr + H(r)(dr)^2 + r^2(d\theta^2 + \sin^2\theta d\phi^2).$$

Since the geometry is at rest we know that the line element should be invariant under the transformation $t \to -t$, however currently this is not the case unless $G(r) = 0$, which gives us:

$$ds^2 = -F(r)dt^2 + H(r)dr^2 + r^2\left(d\theta^2 + \sin^2\theta d\phi^2\right). \tag{25}$$

We know that as $r \to \infty$, $ds^2 \to \eta_{\alpha\beta}dx^\alpha dx^\beta$. Thus:

$$\lim_{r\to\infty}(F) = \lim_{r\to\infty}(H) = 1. \tag{26}$$

Equation (26) gives us some restrictions on the functions $F$ and $H$. However to finally narrow down F and H to specific function requires a diversion into areas

[8] To keep things simple we neglect to change the symbols though the functions are changing.
[9] We again neglect to change the notation.

of tensor calculus that are beyond the scope of this project so I will simply quote the relevant result[10].

The line element which encapsulates Schwarzschild geometry is[11]:

$$ds^2 = -\left(1 - \frac{2M}{r}\right) dt^2 + \left(1 - \frac{2M}{r}\right)^{-1} dr^2 + r^2 \left(d\theta^2 + \sin^2\theta d\phi^2\right) \tag{27}$$

which clearly has the metric:

$$\begin{bmatrix} -\left(1 - \frac{2M}{r}\right) & 0 & 0 & 0 \\ 0 & \left(1 - \frac{2M}{r}\right)^{-1} & 0 & 0 \\ 0 & 0 & r^2 & 0 \\ 0 & 0 & 0 & r^2 \sin\theta \end{bmatrix}. \tag{28}$$

Where $t$ is the time as measured at infinity; $r$ is defined so that the surface area of nested spheres is $4\pi r^2$ like in Euclidean space. However it only gives a precise measure of radial distances in the flat space limit $r \to \infty$; $\theta$ and $\phi$ are angular coordinates as usually defined[12].

## 4.2 Singularities and The Event Horizon

In the coordinate system we have been using it appears that something strange is happening at the points $r = 0$ and $r = 2M$ since at these points the components $g_{00}$ and $g_{11}$ blow up respectively. When this happens it is called a singularity. To complete our understanding of all possible light trajectories we would need to know what was happening at those points. It only affects our understanding of plunge trajectories because both the other kind of trajectory always have $r \geq 3M > 2M$ as we see later in Section 4.5. In this Section we explore these singularities using information sourced from Hartle [1] - Sections 7.1 and 12.1

### Singularities

There are two types of singularity that we are interested in: coordinate singularities and spacetime singularities. A coordinate singularity is merely a property of the coordinate system chosen and does not necessarily correspond to anything physically interesting. Coordinate singularities occur because the chosen coordinate system fails at some points to give a unique label to these points. For example in two-dimensional polars the point $(0, \theta_1) = (0, \theta_2)$ for any angles $\theta_1$ and $\theta_2$. To overcome this problem we use a patchwork of different coordinate systems to cover the region of spacetime we are interested in. Ensuring that the coordinate system we use in any one region does not have any coordinate singularities in that region.

[10] For why this is see Hobson et al. [3] - Section 9.2.

[11] See Hartle [1] - page 189.

[12] For a more detailed discussion of interpretation of the coordinates see Hobson et al. [3] - Sections 11.1 and 11.2.

To show that a singularity is a coordinate singularity we need to find a coordinate system in which the metric is not singular at the relevant points. It is beyond the scope of this project to look at this in any more detail but an understanding of how this is done in Schwarzschild geometry via Eddington-Finkelstein coordinates can be gleaned from, amongst others, Hobson et al. [3] - Section 11.5

A spacetime singularity is a point at which some physical property, i.e. a property that is invariant under coordinate transformations, blows up. It can be shown that tidal effects approach infinity as $r$ approaches zero, showing that the singularity at $r = 0$ is genuine[13].

**The Event Horizon**

Using Eddington-Finkelstein coordinates we can show that it is impossible for light to move from $r < 2M$ to $r > 2M$[14]. This implies that the outside is causally separated from the inside (though not the other way round) and for this reason it is called the event horizon[15]. If we look at the $dt^2$ term in equation (27) we can see that the time as measured from infinity blows up as $r$ approaches $2M$ from the positive side. This means that if we were to observe someone crossing the event horizon we would see them slow asymptotically to a stand still! In this project we only concern ourselves with motion outside of the event horizon.

## 4.3 Null Geodesics In Schwarzschild Geometry

As we wish to understand light trajectories in Schwarzschild geometry we need to work out what restrictions the geodesic equation places on the motion, and also stipulate that the four-velocity is null. This is done in this Section which is based on Chow [2] - Section 4.3 and influenced by Hartle [1] - Chapter 9.

Using Mathematica, or otherwise, from the Geodesic equation (21) with the Schwarzschild metric (28) we calculate the equations of motion for free test particles in a Schwarzschild spacetime as[16]:

$$\ddot{t} = \frac{M\dot{t}\dot{r}}{2Mr - r^2}$$

$$\ddot{r} = \frac{M\dot{t}^2(2M - r)}{r^3} - \frac{M\dot{r}^2}{2Mr - r^2} - \dot{\phi}^2(2M - r)\sin\theta - \dot{\theta}^2(2M - r)$$

$$\ddot{\theta} = \frac{1}{2}\dot{\phi}^2\cos\theta - \frac{2\dot{\theta}\dot{r}}{r}$$

$$\ddot{\phi} = -\frac{\dot{\phi}(r\dot{\theta}\cot\theta + 2\dot{r})}{r}$$

[13] See Hobson et al. [3] - Section 11.2.

[14] See Hartle [1] - Section 12.1.

[15] Though actually when quantum mechanics is taken into account this is not entirely the case and black holes very slowly lose energy and emit particles that influence the outside.

[16] For the Mathematica notebook used see Appendix A. This is an adaptation of a notebook supplied on Hartles website [16].

where $\dot{x}^\alpha = \frac{dx^\alpha}{d\lambda}$ and $\ddot{x}^\alpha = \frac{d^2x^\alpha}{d\lambda^2}$.

We can simplify this immediately by noticing that if we assume that at $\lambda = 0$, $\theta = \pi/2$ and $\dot{\theta} = 0$, the motion now lies in the plane $\theta = \pi/2$. We can do this, without loss of generality, since Schwarzschild geometry is spherically symmetric, ergo we can always rotate our frame of reference so this is the case. Thus the equations become:

$$\ddot{t} = \frac{2M\dot{t}\dot{r}}{2Mr - r^2} \tag{29}$$

$$\ddot{r} = \frac{M\dot{t}^2(2M - r)}{r^3} - \frac{M\dot{r}^2}{2Mr - r^2} - \dot{\phi}^2(2M - r) \tag{30}$$

$$\ddot{\theta} = 0 \tag{31}$$

$$\ddot{\phi} = -\frac{2\dot{\phi}\dot{r}}{r}. \tag{32}$$

If we next focus on equation (32) we can see that it implies:

$$\frac{\ddot{\phi}}{\dot{\phi}} = -\frac{2M\dot{r}}{r} \Rightarrow \frac{d}{d\lambda}\left(\log\dot{\phi}\right) = -2\frac{d}{d\lambda}\left(\log r\right) \Rightarrow \log\dot{\phi} = \log\left(hr^{-2}\right) \Rightarrow \dot{\phi} = \frac{h}{r^2} \tag{33}$$

for some constant of integration h. Similarly from equation (29) we have:

$$\frac{\ddot{t}}{\dot{t}} = \frac{2M\dot{r}}{(2M - r)r} \Rightarrow \frac{d}{d\lambda}\left(\log\dot{t}\right) = \frac{d}{d\lambda}\left(\log\left(1 - \frac{2M}{r}\right)^{-1}\right) \Rightarrow \dot{t} = e\left(1 - \frac{2M}{r}\right)^{-1} \tag{34}$$

for some constant of integration e. If the results of equations (31), (33) and (34) are now plugged into (22) the result becomes:

$$0 = \frac{-e^2}{\left(1 - \frac{2M}{r}\right)} + \frac{\dot{r}^2}{\left(1 - \frac{2M}{r}\right)} + \frac{h^2}{r^2} \tag{35}$$

$$\Rightarrow \dot{r}^2 = e^2 - \frac{h^2\left(r - 2M\right)}{r^3} \tag{36}$$

## 4.4 Symmetry

Unfortunately the coupled second order differential equations given by the Geodesic equations (20) and (21) tend to be intractable in all but the simplest of cases, meaning that it is nigh on impossible to solve them analytically using the standard methods of integration. Though we have managed to do it for Schwarzschild geometry in Section 4.3 this was only because the Schwarzschild case is much simpler than most as there is a high degree of symmetry in its construction. We can use our knowledge of how symmetries affect geodesics to give us additional information that will allow us to construct our first order equations more easily. We can do this since a symmetry implies that some quantity is conserved and we can work out what this quantity is via a 'Killing

vector' named after the German mathematician Wilhelm Killing (1847-1923)[17]. In this section we explore why this is, having sourced information from Hartle [1] - Section 8.2. We then go on to apply this to the Schwarzschild case in a fashion similar to that found in Hartle [1] - Sections 9.3 and 9.4

### Killing Vectors

If we apply equation (13) to a Lagrangian that is independent of a coordinate which, without loss of generality, we say is $x^0$ we get:

$$\frac{d}{d\sigma}\left(\frac{\partial L}{\partial\left(\frac{dx^0}{d\sigma}\right)}\right) = 0 \tag{37}$$

for:

$$L = \left(g_{0\beta}(x)\frac{dx^0}{d\sigma}\frac{dx^\beta}{d\sigma}\right)^{1/2}. \tag{38}$$

This, along with the affine parameter version of equation (12), implies that:

$$\frac{\partial L}{\partial\left(\frac{dx^0}{d\sigma}\right)} = \frac{1}{2L}g_{0\beta}(x)\frac{dx^\beta}{d\sigma} = \frac{1}{2}g_{0\beta}(x)\frac{dx^\beta}{d\lambda} = \text{constant}. \tag{39}$$

Now if we introduce a vector $\xi^\alpha = (1,0,0,0)$, from the scalar product equation (9) and the above we get:

$$\xi\cdot\mathbf{u} = g_{\alpha\beta}\xi^\alpha u^\beta = g_{0\beta}(x)\frac{dx^\beta}{d\lambda} = \text{constant}. \tag{40}$$

We call $\xi$ a Killing vector and it has the associated conserved quantity $g_{0\beta}(x)dx^\beta/d\lambda$. We can have more complicated Killing vectors, which relate to coordinates of which the Lagrangian is not independent, however this is sufficient for our purposes.

### Symmetries in Schwarzschild Geometry

We recall that we constructed the metric (28) so that it had the following two properties.

- Time independence. As the metric does not depend on time the geometry is symmetric with regard to translations in time, with the associated Killing vector $\xi^\alpha = (1,0,0,0)$. This is useful as it means the quantity $e = -\xi\cdot\mathbf{u} = (1-2M/r)\,dt/d\lambda$ is conserved. For sufficiently large values of $r$, $e$ becomes energy per unit mass so in the flat space limit this becomes the conservation of energy.

[17] See J. J. O'Conner et al. [17].

- Spherical symmetry. The metric is clearly independent of $\phi$ and so invariant under rotations about the z-axis, this has the associated Killing vector $\eta^\alpha = (0, 0, 0, 1)$. Other rotational symmetries are less clear but there are associated Killing vectors, however we will not need them. Similarly to the above, this means that $h = \eta \cdot \mathbf{u} = r^2 \sin^2 \theta d\phi/d\lambda$ is conserved. This is the conservation of angular momentum.

Thus we have two conservation laws:

$$e = -\xi \cdot \mathbf{u} = \left(1 - \frac{2M}{r}\right) \frac{dt}{d\lambda} \tag{41}$$

$$h = \eta \cdot \mathbf{u} = r^2 \sin^2 \theta \frac{d\phi}{d\lambda} = r^2 \frac{d\phi}{d\lambda}. \tag{42}$$

Note that $e$ and $h$ are the constants of integration that appeared when we constructed the equations of motion directly in Section 4.3. Further note that $h \geq 0$ for $d\phi/d\lambda \geq 0$, as we can rotate the frame and it makes no difference we can define $h \geq 0$. We also chose our affine parameter $\lambda$ so that $\dot{t} > 0$, since we are dealing with events outside the event horizon (see Section 4.2), this means $r > 2M$ and thus $e > 0$ .

We can now continue, as we did at the end of Section 4.3, to produce equation (36) which rearranges to:

$$\Rightarrow -\left(1 - \frac{2M}{r}\right)^{-1} e^2 + \left(1 - \frac{2M}{r}\right)^{-1} \left(\frac{dr}{d\lambda}\right)^2 + \frac{h^2}{r^2} = 0.$$

Later on we use these symmetries and their associated conservation laws to study the more complicated case of rotating black holes.

## 4.5 Effective potential for Schwarzschild Black Holes

The actual trajectories can only be worked out by integrating the equations of motion - (30) and (32) - numerically, which is how the graphs in this Section have been produced[18]. However we can analyze some of the properties using the quantity $W_{eff}$ that is analogous to the effective potential $V_{eff}$ used to understand the trajectories of massive particles in Schwarzschild geometry[19], and other orbital problems. The discussion that follows is based largely on Hartle [1] - Section 9.4 and Hobson et al. [3] - Section 9.10

It is clear that equation (36) may be rearranged to:

$$\frac{1}{b^2} - W_{eff}(r) = \frac{1}{h^2} \left(\frac{dr}{d\lambda}\right)^2 \tag{43}$$

[18]The Mathematica notebook used can be found in Appendix B and was based on one provided on the accompanying website to Hartle [16] which I adapted from the massive particle to the light case.

[19]See Hartle [1] - Section 9.3.

where:

$$W_{eff}(r) \equiv \frac{1}{r^2}\left(1 - \frac{2M}{r}\right), \text{ and } b \equiv \frac{h}{e} \tag{44}$$

We also have:

$$\frac{1}{h^2}\left(\frac{dr}{d\lambda}\right)^2 \geq 0 \Rightarrow \frac{1}{b^2} \geq W_{eff}(r).$$

This tells us that there is a turning point in $r$ at $1/b^2 = W_{eff}(r)$. We will use this fact to determine the qualitative properties of light ray trajectories. We only consider trajectories that come from $r = \infty$. Obviously $r$ can't actually $= \infty$ in a literal sense, what we mean is that the beginning of the trajectory is sufficiently far away from the mass that the space is approximately flat. Thus we can extend its source arbitrarily further away in a strait line tangential to, and in the opposite direction to, its initial trajectory without it significantly affecting the result, i.e. extend it back to infinity. The circular orbits, which we will see later, can be thought of as coming from infinity before getting trapped into the orbit. Nonetheless, for aesthetic reasons, only the circular part of the orbit is shown in the trajectory graphs. However before we do this it is informative for us to find a physical interpretation of the quantity $b$ introduced earlier in this section. Wel do this in the next section taking guidance from Hobson et al. [3] - Section 9.13.

### 4.5.1 Interpreting b

From equations (36), (42) and our definition of $b$ we have:

$$\frac{d\phi}{dr} = \frac{\dot{\phi}}{\dot{r}} = \frac{b}{r^2\left(1 - \frac{b^2}{r^2}\left(1 - \frac{2M}{r}\right)\right)^{1/2}}$$

$$\Rightarrow r^2\frac{d\phi}{dr} = \frac{b}{\left(1 - \frac{b^2}{r^2}\left(1 - \frac{2M}{r}\right)\right)^{1/2}}$$

Thus

$$\lim_{r\to\infty} r^2\frac{d\phi}{dr} = \pm b$$

Spherical symmetry means we are free to stipulate, without loss of generality, that:

$$\lim_{r\to\infty} \phi = 0.$$

Thus we have, at $r = \infty$:

$$b = r\sin\phi.$$

We are now in a position to offer an interpretation of $b$. It is the distance between the origin (the location of the mass) and what would have been the closest part of the trajectory were the space flat everywhere i.e $b$ is an impact parameter. As shown in Figure 2.

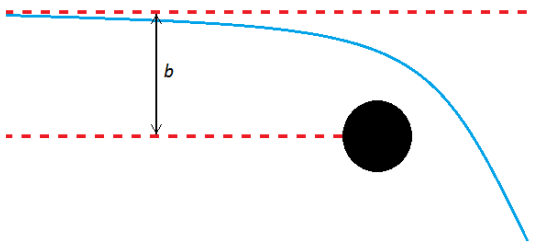


Figure 2: represents the impact parameter $b$ as the distance between the origin and the point of closest approach of the line tangential to the lights initial trajectory.

### 4.5.2 Plotting $W_{eff}$

We next wish to plot $W_{eff}$ against $r$ so that we can compare it with $b$. Differentiating equation (44) we get:

$$\frac{d}{dr}W_{eff}(r) = \frac{2}{r^3}\left(\frac{3M}{r} - 1\right).$$

This implies that the only turning point of $W_{eff}$ is at $r = 3M$. We also have:

$$W_{eff}(3M) = \frac{1}{27M^2}, \quad \frac{d^2}{dr^2}W_{eff}(3M) = -\frac{2}{82M^4} < 0$$

$$\Rightarrow \max W_{eff}(r) = \frac{1}{27M^2} \text{ at } r = 3M.$$

If we now take the limits:

$$\lim_{r\to\infty}(W_{eff}) = 0 \quad \text{and} \quad \lim_{r\to 0}(W_{eff}) = -\infty$$

we can see that we get something that looks like Figure 3. Though in fact here we plot $M^2W_{eff}$ against $r/M$ so that it is scaled correctly. It is possible to remove the explicit $h$ dependence in equation (43) by transforming the affine parameter $\lambda$ which is why we neglect to scale by it in later graphs[20].

### 4.5.3 Plunge Orbits

Let us first consider a light ray with $b < 3\sqrt{3}M$. By plotting $1/b^2$ on to our $W_{eff}$ graph we get Figure 4.

If we imagine a photon is approaching the central mass from $r = \infty$, along the red arrow that represents the value of $b$, we know that $\exists\ \lambda_0$ such that:

$$\frac{dr(\lambda_0)}{d\lambda} < 0.$$

We can see from equation (43) that this implies $dr/d\lambda < 0\ \forall\ \lambda$, since $dr/d\lambda$ is continuous and $dr/d\lambda \neq 0\ \forall\ \lambda$. Thus we get the plunge orbit shown in Figure 5.

[20] See Hobson et al. [3] - Page 220

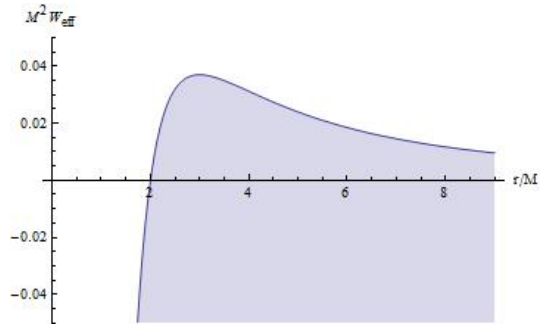


Figure 3: Here we see how $W_{eff}$ varies with $r$. To ensure that it is scaled correctly we actually plot $M^2 W_{eff}$ against $r/M$. Note that the peak, at $r = 3M$, is the only turning point.

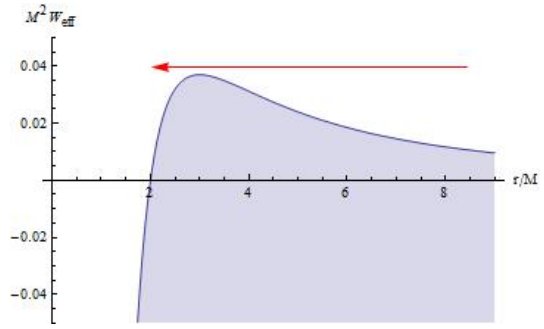


Figure 4: Here we see the graph of $W_{eff}$ in Figure 3 with the value of $1/b^2$ indicated (red arrow). We can see that, since $W_{eff}$ and $1/b^2$ are never equal, there are no turning points in $r$ and so a plunge orbit shown in Figure 5 is inevitable.

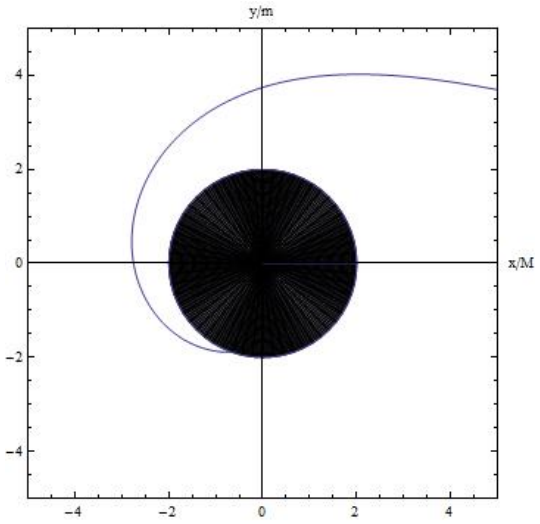


Figure 5: Here we have a plunge orbit indicative of an impact parameter such that $b < 3\sqrt{3}M$. The actual value of $b$ used was $5M$ as indicated in Figure 4. As with previous graphs the axes have been scaled by a factor of $1/M$ to remove their dependence on $M$

#### 4.5.4 Scatter Orbits

We now consider the case where $b$ is such that $b > 3\sqrt{3}M$. Plotting this as before we get Figure 6.

Since $b > 3\sqrt{3}M$ we have $1/b^2 = W_{eff}(r(\lambda_1))$ for some $\lambda_1$. Thus we have:

$$\frac{dr(\lambda_1)}{d\lambda} = 0. \tag{45}$$

By plugging equations (33), (34) and (36) into (30) and simplifying, we produce:

$$\frac{d^2r}{d\lambda^2} = \frac{h^2(3M - r)}{r^3}. \tag{46}$$

This implies that $r(\lambda_1)$ is a local minimum since we know that $\ddot{r} < 0$ as $r > 3M$. We know $r$ then tends back to $\infty$, along the black line, as there are no more turning points in $r$. This scattering orbit, illustrated in Figure 7, is the effect that leads to gravitational lensing discussed in Section 5.

#### 4.5.5 Circular Orbits

The only possible value of the impact parameter not already considered is $b = 3\sqrt{3}M$ which gives Figure 8.

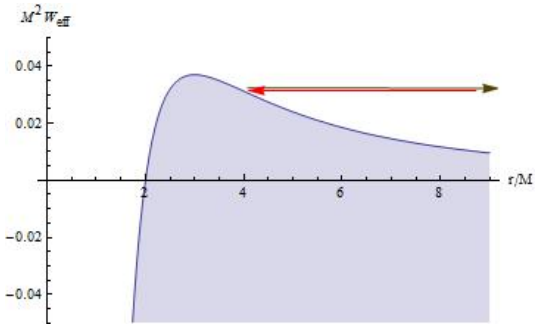


Figure 6: Here we see the graph of $W_{eff}$ in Figure 3 with a new value of $1/b^2$ indicated (red/black arrows). We can see that $W_{eff}$ and $1/b^2$ are equal at a single point thus there is a minima of $r$ at that point. Consequently we get the scatter orbit shown in Figure 7

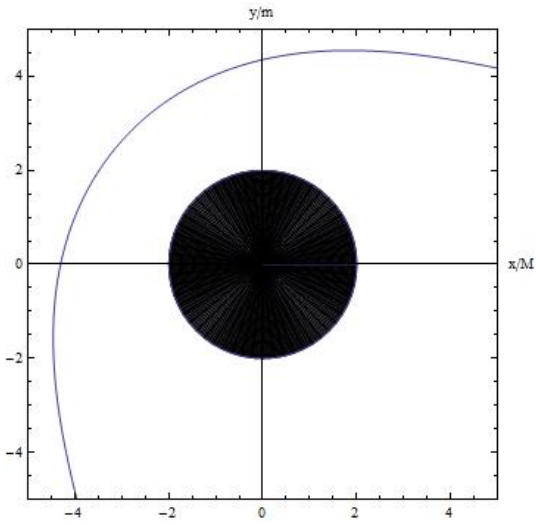


Figure 7: For $b > 3\sqrt{3}M$ we get an orbit similar to the scatter orbit shown above. The actual value of $b$ used was $5.65M$, as indicated in Figure 6. As with previous graphs the axes have been scaled by a factor of $1/M$ to remove their dependence on $M$

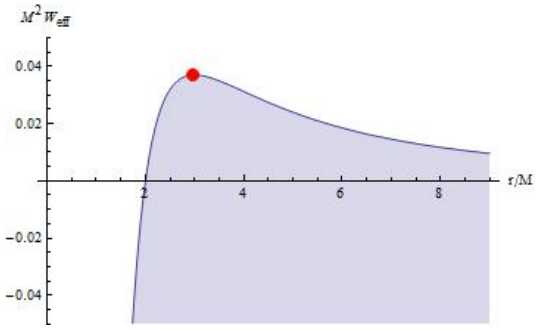


Figure 8: Here we have the limiting case between the scatter and plunge orbits. We see that since $W_{eff} = 1/b^2$ everywhere we get the circular orbit shown in Figure 9

Since $dr/d\lambda_0 = 0$ and $d^2r/d\lambda_0^2 = 0 \Rightarrow r = 3M \ \forall\lambda$ and therefore the trajectory is circular, as in Figure 9. However we can see in Figure 8 that this is unstable, since a small change in one of the parameters will cause the trajectory to become either a plunge or a scatter.

The set of all such circular orbits is called the photon sphere. Since the circular orbits only occur at $r = 3M$ the photon sphere is a property that can only belong to bodies with a radius less than $3M$. If we calculate the radius of the Sun we get[21]:

- Solar mass $\approx 1.989 \times 10^{30}$kg$\approx \frac{6.673\times10^{-11}\times1.989\times10^{30}}{2.998^2\times10^{16}}$m$\approx 1.477$km
- Solar radius $\approx 695500$km$\gg 3 \times 1.477$km.

Showing that our star is far too big to have a photon sphere. If we look at the typical values for a Neutron Star, which is the densest type of star other than a black hole, we get something like:

- Mass $\approx 2$km
- Radius $\approx 12$km$> 3 \times 2$km

which again is too big[22]. Having studied the literature it seems there is little consensus as to whether or not a neutron star of sufficient density to possess a photon sphere is possible in nature. It is certain that all neutron stars have $r > 2M$, as if one didn't it would have an event horizon and so by definition would be a black hole. However a detailed discussion of high density physics is beyond the scope of this project, if you wish to pursue it further see Leung et al. [12]. We can however be certain that photon spheres are not possible for any

[21] Numerical values found using Wolfram Alpha and, though all are given to four significant figures, the calculations have been done with eight significant figures.

[22] Numerical values sourced from Nemiroff [11] - Page 12.

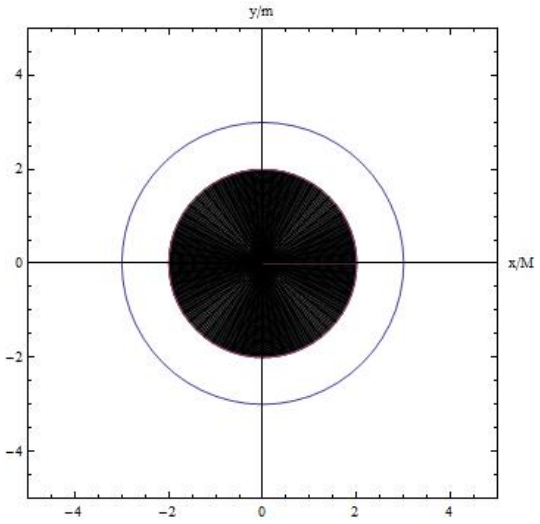


Figure 9: This is a representation of the unstable circular orbit produced by $b = 3\sqrt{3}M$. Again the axes have been scaled

other type of star as white dwarfs are insufficiently dense and all other types less dense still.

# 5 Gravitational Lensing

Light rays, with scattered trajectories (see Section 4.5.4), make their source appear to be in a different part of the sky to where it actually is. This section will explore this phenomenon primarily using information found in Hartle [1]- Sections 9.4 and 11.1 and Hobson et al. [3] - Section 10.2. The discussion has also been informed by Cohen [5] which offers a fairly non-mathematical discussion.

The scattering effect led to one of the earliest tests of general relativity. In 1919 Arthur Edington measured the apparent position of a star close to the Sun during a solar eclipse. He compared this to its relative position six months earlier, and found the difference to be within the margin of error of the predictions made using the Schwarzschild solutions to Einstein's equations.

Though the deflections made by the Sun were tiny, bodies such as black holes or galaxies cause much larger distortions. In fact you can see several images of the same star going round large gravitating bodies in different directions, as is shown in Figure 10. We can get a feeling for why this is by considering Figure 11. This Figure represents our four-dimensional spacetime as a two-dimensional manifold that is curved in the third Euclidean dimension; thus causing the light to bend both ways around the galaxy to the observer. In

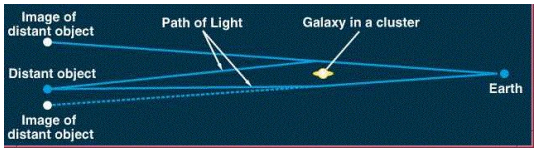


Figure 10: This Figure illustrates gravitational lensing. We can see how scatter orbits make objects appear to be in a different place to where they actually are. This means that light from a single distant object can travel around a mass in multiple directions to the observer, thus producing multiple images. This effect is known as gravitational lensing and is illustrated above
Source: Smith [18]

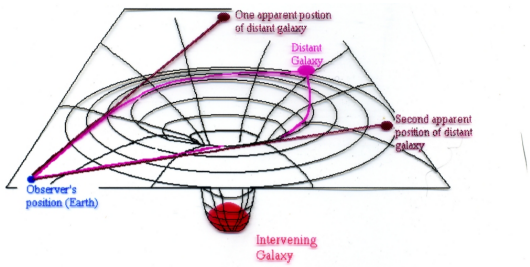


Figure 11: In this Figure our four-dimensional spacetime is represented as a two-dimensional manifold which is curved in the third Euclidean dimension thus causing the light to bend both ways around the galaxy to the observer.
Source: Washington University of St. Louis [19]

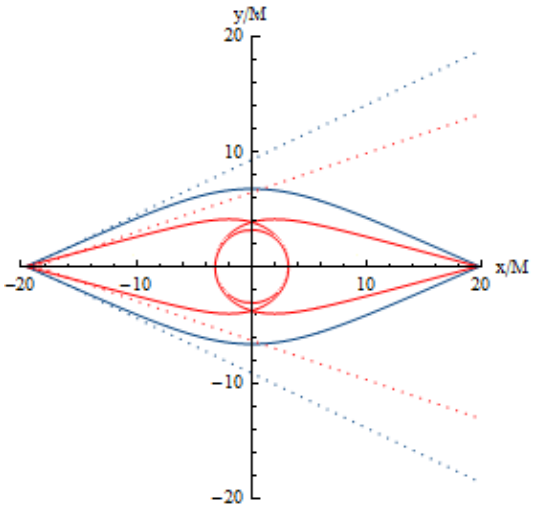


Figure 12: In this figure we see the trajectories taken by light that forms a cross-section of the first (blue) and second (red) Einstein rings. The apparent position of the source is indicated with dotted lines. We can see that the second ring lies inside the first, and by the same process we can show that each successive ring appears within the other but external to the photon sphere.

the diagram there are only two distinct images of the distant galaxy as we are working with a two-dimensional space. In reality, since we have three spatial dimensions, the light can bend round the mass in all directions and so can produce several images. In fact if the object and observer are perfectly aligned with a suitably large mass then they produce a continuous circular image of the object known as an Einstein ring. Inside this first Einstein ring there will be another ring corresponding to light that has completely orbited the mass before traveling on to the observer. Inside this there will be another which consists of of photons that have completed two orbits, and so on ad infinitum[23]. The limiting angular radius of the rings is that of the photon sphere as the trajectories move ever closer to it. These rings become progressively less bright. This is because the required precision, such that the photons trajectory finishes at the observers eye, increases. A cross-section of the first two rings is given in Figure 12. Experimental evidence of Einstein rings has been found, thus adding further credence to General Relativity theory[24]. The image in Figure 13 is from the Hubble telescope and is believed to be an example of an Einstein ring.

[23]For a more detailed discussion of these inner rings, as well as other optical properties of extreme gravity, see Nemiroff [11].

[24]See Warren et al. [8].

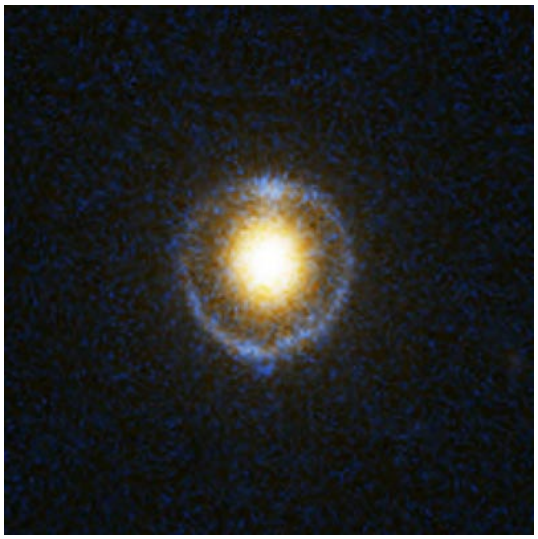

Figure 13: This image is of a candidate Einstein ring was taken by the Hubble telescope [20]

## 5.1 Calculating the Angle of Deflection

We are interested in knowing how much a system will deflect the trajectory of light, or, more usefully, calculating properties of the system based on our measurements of the deflection of light[25]. To calculate this we start by rearranging equation (43) to:

$$\frac{dr}{d\lambda} = \pm h\sqrt{\frac{1}{b^2} - W_{eff}(r)} \tag{47}$$

as can been seen in Hartle [1] - Section 9.4 [The deflection of light] which this Section follows closely. Using the aforementioned equation, $\theta = \pi/2$, equation (42) and the chain rule we get:

$$\frac{d\phi}{dr} = \frac{d\phi}{d\lambda}\Big/\frac{dr}{d\lambda} = \frac{\pm 1}{r^2\sqrt{\frac{1}{b^2} - W_{eff}(r)}}. \tag{48}$$

Since we are not interested in the direction of travel we are free to drop the $\pm$ in the above expression. So the total change in $\phi$ ($\Delta\phi$) is given by:

$$\Delta\phi = \int_{-\infty}^{\infty} \frac{dr}{r^2\sqrt{\frac{1}{b^2} - W_{eff}(r)}}, \tag{49}$$

[25] For a discussion of some of the astronomical applications of gravitational lensing see Ehlers et al. [7] - Section 4.

which, by symmetry, is equal to:

$$2\int_{r_0}^{\infty} \frac{dr}{r^2\sqrt{\frac{1}{b^2} - W_{eff}(r)}} \tag{50}$$

for $W_{eff}(r_0) = 1/b^2$, i.e. $r_0$ is the minimum value of $r$. We can now see that $\Delta\phi$ only depends on $M/b$ since the only other parameter in equation (50) is $r_0$ and that also solely depends on $M/b$. For large $M/b$ we can use numerical methods to solve equation (50). However if $M/b$ is small then we can use perturbation theory to get a good approximation. We do this in the following Section using information sourced from Section 10.2 of Hobson et al. [3]

### 5.1.1 Calculating Small Deflections

We can rearrange the positive part of equation (48) to:

$$\frac{dr}{d\phi} = r^2\sqrt{\frac{1}{b^2} - \frac{1}{r^2}\left(1 - \frac{2M}{r}\right)}. \tag{51}$$

If we then do the substitution $r = \frac{1}{u}$ we get:

$$\frac{du}{d\phi} = \sqrt{\frac{1}{b^2} - u^2\,(1 - 2Mu)}. \tag{52}$$

This differentiates to:

$$\frac{d^2u}{d\phi^2} + u = 3Mu^2. \tag{53}$$

The vacuum solution ($M = 0$) to equation (53) gives:

$$u = A\sin\phi + B\cos\phi.$$

Now plugging in our initial conditions for a photon moving parallel to the $x$ axis with an impact parameter $b$ we get:

$$y = r\sin\phi = b \Rightarrow u = \frac{\sin\phi}{b}.$$

We expect a small mass to give a small perturbation $\delta u$ to the zeroth-order massless case and are free to ignore the higher order terms. So we write:

$$u = \frac{\sin\phi}{b} + \delta u. \tag{54}$$

Plugging this into equation (53) and dropping higher order terms we get:

$$\frac{d^2u}{d\phi^2} + u = -\frac{\sin\phi}{b} + \frac{d^2\delta u}{d\phi^2} + \frac{\sin\phi}{b} + \delta u = 3M\left(\frac{\sin\phi}{b} + \delta u\right)^2 \approx \frac{3M}{b^2}\sin^2\phi \tag{55}$$

which implies:

$$\frac{d^2\delta u}{d\phi^2} + \delta u \approx \frac{3M}{b^2}\sin^2\phi. \tag{56}$$

Solving this we get :

$$\delta u \approx \frac{M}{b^2}\left(3 + \cos 2\phi\right). \tag{57}$$

Plugging this into equation (54) and taking the limit as $r \to \infty$ we get:

$$\lim_{r\to\infty} \frac{\sin\phi}{b} + \frac{M}{b^2}\left(3 + \cos 2\phi\right) = \frac{\phi}{b} + \frac{4M}{b^2} \approx 0 = \lim_{r\to\infty} u. \tag{58}$$

This gives:

$$\phi \approx -4\frac{M}{b}. \tag{59}$$

Thus the angle of deflection, in standard SI units, for $M \ll b$ is given by:

$$\Delta\phi \approx \frac{4GM}{c^2 b}. \tag{60}$$

### 5.1.2 Light Deflection by the Sun

We now apply this to the Sun, as Arthur Eddington did for his famous experiment of 1919, using the values given in Section 4.5.5. For a light ray passing as close as possible to the Sun we take the minimum value of $r$ ($r_0$) to be the solar radius 695500km. We take the solar mass, as before, to be 1.477km. Via the equation $W_{eff}(r_0) = 1/b^2$, we calculate the value of $b$ to be $b \approx 695500$km and so we get[26]:

$$\Delta\phi \approx \frac{4 \times 1.477}{695500} \approx 8.493 \times 10^{-6}\text{radians} \approx 1.752".$$

The angle of deflection is very small and so it created quite a challenge for Eddington to measure. The values he got from his two separate sets of measurement were $\Delta\phi = 1.98" \pm 0.16"$ and $1.61" \pm 0.4$[27]. These where considered to be sufficiently consistent with the theory to provide the first confirmation of a prediction made using Einstein's General Relativity theory. We would not expect the measured value to exactly equal the predicted value, even if we could remove experimental error and equation (60) was exact, since the Sun is a non-isolated, rotating body which is only approximately symmetric, and therefore the geometry is only approximated by Schwarzschild. However these measurements, and much more accurate ones made since, confirm that it is a reasonably accurate model. We are next going to use our deflection angle approximation to construct an equation that allows us to derive the approximate mass of celestial bodies.

[26] Numerical values are all given to four significant figures and the calculations have been done with eight significant figures as before.

[27] Numerical values found in Hobson et al. [3] - top of page 235.

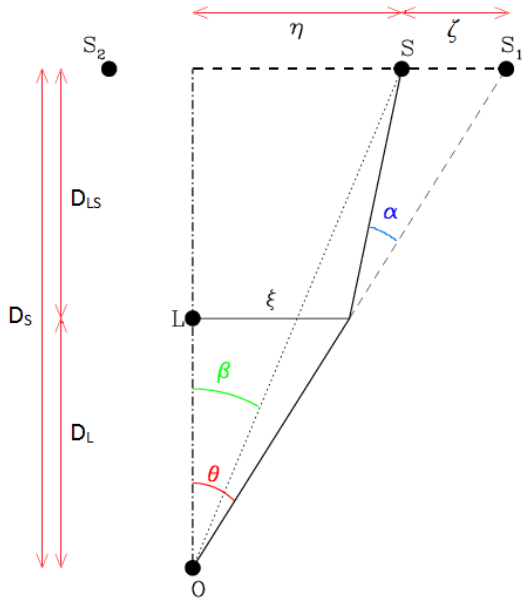


Figure 14: In this diagram the observer is placed at the origin, the lens at $L$ and the light source at $S$. We can see the two images that the light source produces for the observer at $S_1$ and $S_2$. The distances and angles between these points are also indicated. This Figure is an adaptation of one found in Wambsganss [22]

### 5.1.3 The Thin Lens Approximation

To simplify things we are only going to consider gravitational lensing in a geometry with a single spherically symmetric source of curvature, i.e. Schwarzschild geometry. We will assume the mass to be at a point and all of the light deflection to occur instantaneously in the plane of normals to the line of site of the lens, at the lens (in Figure 14 this is the plane that would result from rotating $\xi$ about the $0 - L$ axis and extending to infinity). Our final assumption is that the deflection angle is given exactly by equation (60). This approximation is accurate when the $b \gg M$ and when the distances between the observer, lens and source are much greater than the size of the lens itself. This last requirement is almost always true when dealing with observable astronomical objects. For a more detailed discussion of some of the properties of gravitational lenses and how they relate to real world observations see Hartle [1] - Section 11.1, the material at the beginning of which informed this Section.

In Figure 14 the observer is placed at the origin, the lens at $L$ and the light source at $S$. We can see the two images that the light source produces for the observer at $S_1$ and $S_2$. The distances and angles between these points are also

indicated. To simplify our notation we have replace $\Delta\phi$ with $\alpha$ in equation (60).

Our assumptions imply that $D_s \gg \eta + \zeta$ so we have, to a good approximation:

$$\eta \approx \beta D_S, \quad \zeta \approx \alpha D_{LS}, \quad \eta + \zeta \approx \theta D_S, \quad b \approx \xi \approx \theta D_L$$

We assume this approximation holds to sufficient accuracy for our purposes and we get the lens equation:

$$\theta D_S = \beta D_S + \alpha D_{LS}. \tag{61}$$

Plugging in our value for $\alpha$ from equation (60) we get:

$$\theta D_S = \beta D_S + 4\frac{M}{b} D_{LS} = \beta D_S + 4\frac{M}{\theta D_L} D_{LS}.$$

We now rearrange to get:

$$\theta = \beta + 4M\frac{D_{LS}}{\theta D_L D_S}. \tag{62}$$

It is easy to see that the above equation allows us to calculate the mass ($M$) of the lens simply by measuring the angles $\beta$ and $\theta$ when the values of $D_L$ and $D_S$ have been calculated via other means.

We can also use equation (62) to glean an understanding of Einstein rings discussed in the introduction of this Section. Though in some cases our approximation is not very accurate. Clearly if the source, lens and observer are aligned then the angle $\beta = 0$ giving:

$$\theta^2 = 4M\frac{D_{LS}}{D_L D_S} \Rightarrow \theta = \pm 2\sqrt{M\frac{D_{LS}}{D_L D_S}}$$

Thus in this plane images appear in the two positions that are an angle $2\sqrt{MD_{LS}/D_L D_S}$ from the observer, lens, source axis. The symmetry of the situation is such that this is true for all planes that are rotations of our starting plane about this axis. Thus we get a ring of images around the lensing mass with a radius of approximately $2\sqrt{MD_S D_{LS}/D_L}$.

# 6 Light Orbits in the Equatorial Plane of Kerr Black Holes

Rotating black holes, known as Kerr black holes, have two parameters that completely determine their properties. These are the black hole's angular momentum ($J$) and, as with the Schwarzschild case, mass ($M$). This Section will discuss how rotation affects light trajectories in the equatorial plane of Kerr black holes. We start with a discussion of the Kerr line element and metric which is based on Hartle [1] - Section 15.2 and Hobson et al. [3] - Section13.5.

## 6.1 Kerr Metric and Line Element

For a suitable set of coordinates, called Boyer-Lindquist Coordinates (see Section 6.2), the line element that describes the geometry outside rotating masses is[28]:

$$ds^2 = -\left(1 - \frac{2Mr}{r^2 + \frac{J^2}{M^2}\cos^2\theta}\right)dt^2 - \frac{4Jr\sin^2\theta}{r^2 + \frac{J^2}{M^2}\cos^2\theta}d\phi dt + \frac{r^2 + \frac{J^2}{M^2}\cos^2\theta}{r^2 - 2Mr + \frac{J^2}{M^2}}dr^2$$
$$+\left(r^2 + \frac{J^2}{M^2}\cos^2\theta\right)d\theta^2 + \left(r^2 + \frac{J^2}{M^2} + \frac{\frac{2J^2r}{M}\sin^2\theta}{r^2 + \frac{J^2}{M^2}\cos^2\theta}\right)\sin^2\theta d\phi^2 \qquad (63)$$

which, as one would expect, reduces to the Schwarzschild line element (27) for the case $J = 0$.

To keep things simple we are only going to look at motion restricted to the equatorial plane, i.e. $\theta = \pi/2$ and $d\theta/d\lambda = 0$. It so happens that, in general, geodesics in Kerr geometry do not lie in a plane, however equatorial orbits do[29].

To simplify our notation we introduce the angular momentum per unit mass $a \equiv J/M$ and the quantity $\Delta \equiv r^2 - 2Mr + a^2$. Applying these simplifications to the line element (63) it reduces to:

$$ds^2 = -\left(1 - \frac{2M}{r}\right)dt^2 - \frac{4aM}{r}d\phi dt + \frac{r^2}{\Delta}dr^2 + \left(r^2 + a^2 + \frac{2a^2M}{r}\right)d\phi^2. \quad (64)$$

With the corresponding metric:

$$\begin{bmatrix} -\left(1 - \frac{2M}{r}\right) & 0 & 0 & -\frac{2aM}{r} \\ 0 & \frac{r^2}{\Delta} & 0 & 0 \\ 0 & 0 & 0 & 0 \\ -\frac{2aM}{r} & 0 & 0 & \left(r^2 + a^2 + \frac{2a^2M}{r}\right) \end{bmatrix} \qquad (65)$$

## 6.2 Boyer-Lindquist Coordinates

The coordinates we are using are not the same as Schwarzschild coordinates used in earlier Sections. Unfortunately the coordinates we use, called Boyer-Lindquist Coordinates, do not lend themselves so easily to geometrical interpretation as Schwarzschild coordinates. Nonetheless, in this Section, we will look at some properties of this coordinate system. This discussion of Boyer-Lindquist coordinates is based on Hobson et al. [3] - Section 13.6. The original paper describing this coordinate system can be found in Boyer et al. [9] which is more complete and more technically demanding. This paper has also informed this Section.

If we now consider the limit of the Kerr line element (63), as $M \to 0$, we see that we get:

[28] For a discussion of how this line element can be derived see Hobson et al. [3] - Sections 13.1, 13.5 and 13.7.

[29] See Hobson et al. [3] - Section 13.10.

$$ds^2 = -dt^2 + \frac{r^2 + a^2\cos^2\theta}{r^2 + a^2}dr^2 + \left(r^2 + a^2\cos^2\theta\right)d\theta^2 + \left(r^2 + a^2\right)\sin^2\theta d\phi^2$$

Now we expect this to be Minkowski spacetime. And indeed one can show without too much difficulty that applying the transformation below gives the flat line element.

$$\begin{aligned} t &= t \\ x &= \sqrt{r^2 + a^2}\sin\theta\cos\phi \\ y &= \sqrt{r^2 + a^2}\sin\theta\sin\phi \\ z &= r\cos\theta \end{aligned}$$

where $(t, x, y, z)$ are ordinary Cartesian coordinates. As we are only going to be dealing with the equatorial plane this becomes:

$$\begin{aligned} t &= t \\ x &= \sqrt{r^2 + a^2}\cos\phi \\ y &= \sqrt{r^2 + a^2}\sin\phi \\ z &= 0 \end{aligned}$$

and we can see that for $a = 0$ these are just ordinary polar coordinates. The above interpretation can be misleading for $M \neq 0$ however it does allow us to highlight a key way in which Kerr spacetime differs from the Schwarzschild case which we do in the next Section.

## 6.3 Singularities in Kerr Geometry

Inspection of the line element (63) reveals that, in Boyer-Lindquist coordinates, it is singular at $r^2 + a^2\cos^2\theta = 0$ and $\Delta = 0$. This section discusses these singularities, basing the account on Hobson et al. [3] - Sections 13.4, 13.6 and 13.8, Boyer et al. [9] and, to a lesser extent, Hartle [1] - Section 15.3.

The Singularity at $r^2 + a^2\cos^2\theta = 0$ is real and occurs at $r = 0$ and $\theta = \pi/2$ (i.e. in the equatorial plane). Following the earlier precedent of this document we will not discuss in any detail what happens inside the event horizon(s) of the black hole and so we will not look at this singularity in any detail. However we note that, from our discussion in Section 6.2, this singularity forms a ring of radius $a$ rather than a point.

The second set of singularities, the solutions to $\Delta = 0$, are coordinate singularities. They are the solutions to $r^2 - 2Mr + a^2 = 0$ which clearly are:

$$r_\pm = M \pm \sqrt{M^2 - a^2}. \tag{66}$$

It can be shown that both of these solutions correspond to event horizons[30]. It is also worth noting that there are no real solutions to $\Delta = 0$ for $a^2 > M^2$.

[30] To see how this is done see Hobson et al. [3] - Section 13.4.

If this situation is possible it would mean that the ring singularity would be naked, i.e trajectories could come infinitesimally close to it before returning to $\infty$. However there are reasons to believe that this situation is impossible in nature, and for this reason we ignore it[31].

Thus we have seen that the structure of Kerr black holes is significantly different to that of Schwarzschild, having a ring singularity and 2 event horizons. It can be further shown that the Kerr case has another boundary called the Ergosphere, which lies at $r = 2M$ in the equatorial plane. In the region bound by the Ergosphere it is impossible for an object to remain at rest with respect to $\infty$, we did not need to draw the distinction between the event horizon and Ergosphere in our Schwarzschild discussion since for $a = 0$ both occur at $r = 2M$ and $r = 0$.

## 6.4 Symmetries of Kerr Geometry

Since the metric (65) does not depend on the coordinates $t$ and $\phi$ we have two Killing vectors and their associated conservation laws. This section derives a first order, ODE in $r$ from these conservation laws, basing the discussion on Hobson et al. [3] - Section 13.10 and Boyer et al. [9].

Our Killing vectors and associated conservation laws are:

$$\xi = (1,0,0,0), \quad \xi \cdot \mathbf{u} = g_{0\beta}(x)\frac{dx^\beta}{d\lambda} = -\left(1 - \frac{2M}{r}\right)\frac{dt}{d\lambda} - \frac{2aM}{r}\frac{d\phi}{d\lambda} = -e$$

$$\eta = (0,0,0,1), \quad \eta \cdot \mathbf{u} = g_{4\beta}(x)\frac{dx^\beta}{d\lambda} = -\frac{2aM}{r}\frac{dt}{d\lambda} + \left(r^2 + a^2 + \frac{2a^2M}{r}\right)\frac{d\phi}{d\lambda} = h.$$

Giving the matrix equation:

$$\begin{bmatrix} -\left(1 - \frac{2M}{r}\right) & -\frac{2aM}{r} \\ -\frac{2aM}{r} & \left(r^2 + a^2 + \frac{2a^2M}{r}\right) \end{bmatrix} \begin{bmatrix} \frac{dt}{d\lambda} \\ \frac{d\phi}{d\lambda} \end{bmatrix} = \begin{bmatrix} -e \\ h \end{bmatrix}. \tag{67}$$

Solving (67) we get:

$$\begin{bmatrix} \frac{dt}{d\lambda} \\ \frac{d\phi}{d\lambda} \end{bmatrix} = \frac{-1}{\Delta} \begin{bmatrix} \left(r^2 + a^2 + \frac{2a^2M}{r}\right) & \frac{2aM}{r} \\ \frac{2aM}{r} & -\left(1 - \frac{2M}{r}\right) \end{bmatrix} \begin{bmatrix} -e \\ h \end{bmatrix} \tag{68}$$

i.e.

$$\frac{dt}{d\lambda} = \frac{1}{\Delta}\left(\left(r^2 + a^2 + \frac{2a^2M}{r}\right)e - \frac{2aM}{r}h\right) \tag{69}$$

$$\frac{d\phi}{d\lambda} = \frac{1}{\Delta}\left(\frac{2aM}{r}e + \left(1 - \frac{2M}{r}\right)h\right). \tag{70}$$

As we are still interested in the trajectories of light, we are still dealing with null geodesics, therefore equation (22) still applies. Plugging our conservation laws and the equatorial Kerr metric (65) into equation (22) we get:

[31] For a discussion of this conjecture, known as cosmic censorship, see Hartle [1] - Section 15.1.

$$\mathbf{u}\cdot\mathbf{u}= g_{\alpha\beta}\left(x\right)\frac{dx^{\alpha}}{d\lambda}\frac{dx^{\beta}}{d\lambda}=$$

$$-\left(1-\frac{2M}{r}\right)\left(\frac{dt}{d\lambda}\right)^{2}-\frac{4aM}{r}\frac{d\phi}{d\lambda}\frac{dt}{d\lambda}+\frac{r^{2}}{\Delta}\left(\frac{dr}{d\lambda}\right)^{2}+\left(r^{2}+a^{2}+\frac{2a^{2}M}{r}\right)\left(\frac{d\phi}{d\lambda}\right)^{2}=$$

$$-\left(1-\frac{2M}{r}\right)\left(\frac{1}{\Delta}\left(\left(r^{2}+a^{2}+\frac{2a^{2}M}{r}\right)e-\frac{2aM}{r}h\right)\right)^{2}$$

$$-\frac{4aM}{r}\frac{1}{\Delta^{2}}\left(\frac{2aM}{r}e+\left(1-\frac{2M}{r}\right)h\right)\left(\left(r^{2}+a^{2}+\frac{2a^{2}M}{r}\right)e-\frac{2aM}{r}h\right)$$

$$+\frac{r^{2}}{\Delta}\left(\frac{dr}{d\lambda}\right)^{2}+\left(r^{2}+a^{2}+\frac{2a^{2}M}{r}\right)\left(\frac{1}{\Delta}\left(\frac{2aM}{r}e+\left(1-\frac{2M}{r}\right)h\right)\right)^{2}=0.$$

As we are dealing with $r>r_{+}$ we are free to multiply by $-\Delta/(rh)^{2}$ and take the $dr/d\lambda$ term to the other side, giving:

$$\frac{1}{\Delta r^{2}}\left(1-\frac{2M}{r}\right)\left(\left(r^{2}+a^{2}+\frac{2a^{2}M}{r}\right)\frac{\sigma}{b}-\frac{2aM}{r}\right)^{2}$$

$$+\frac{4aM}{r}\frac{1}{\Delta r^{2}}\left(\frac{2aM}{r}\frac{\sigma}{b}+\left(1-\frac{2M}{r}\right)\right)\left(\left(r^{2}+a^{2}+\frac{2a^{2}M}{r}\right)\frac{\sigma}{b}-\frac{2aM}{r}\right)$$

$$-\frac{1}{\Delta r^{2}}\left(r^{2}+a^{2}+\frac{2a^{2}M}{r}\right)\left(\frac{2aM}{r}\frac{\sigma}{b}+\left(1-\frac{2M}{r}\right)\right)^{2}=\frac{1}{h^{2}}\left(\frac{dr}{d\lambda}\right)^{2}$$

for $\sigma=ha/\|ha\|$ restoring the condition $h>0$, and giving the condition $a>0$[32], i.e. $\sigma$ is one if the orbit is in the same direction as the rotation of the mass (corotating/prograde) or minus one if it is rotating in the opposite direction (counterrotating/retrograde). This simplifies to:

$$\frac{1}{h^{2}}\left(\frac{dr}{d\lambda}\right)^{2}=\frac{1}{b^{2}}-W_{eff}(r,b,\sigma) \tag{71}$$

for:

$$W_{eff}(r,b,\sigma)=\frac{1}{r^{2}}\left[1-\left(\frac{a}{b}\right)^{2}-\frac{2M}{r}\left(1-\sigma\frac{a}{b}\right)^{2}\right]. \tag{72}$$

We can now perform an analysis similar to that performed in Section 4.5 to determine the shape of our orbits. However now we have two parameters, $(b,\sigma)$ or, if you like, $(h,e)$ which determine the trajectory around a Kerr black hole, of given mass and angular momentum. We can also see that for $a=0$ equation (72) reduces to (44) as required.

[32]Clearly we can only stipulate that $h$ and $a$ are positive once we have determined $\sigma$.

## 6.5 Effective Potential for Kerr Black Holes

As we saw in Section 4.5, the actual trajectories can only be calculated numerically[33]. In order that we may continue an analytical discussion we will study the turning points of $r$, as given by equation (71), to give us some understanding of the trajectories. To do this we base our discussion on Hobson et al. [3] - Sections 13.15, 13.16, 13.17 and 13.18. This section has also been informed by O'Neill [6] - Section 4.14.

From equation (72) we get:

$$\frac{d}{dr}W_{eff}(r) = \frac{2}{r^3}\left(\frac{3M}{r}\left(1-\sigma\frac{a}{b}\right)^2 + \left(\frac{a}{b}\right)^2 - 1\right).$$

This implies that the value of $r$ for which $W_{eff}$ is maximal ($r_c$) is given by:

$$\frac{d}{dr}W_{eff}(r_c) = 0$$

$$\Rightarrow r_c = \frac{3M\left(1-\sigma\frac{a}{b}\right)^2}{1-\left(\frac{a}{b}\right)^2} = \frac{3M(b-\sigma a)}{b+\sigma a}. \tag{73}$$

At this point $W_{eff}$ takes the value:

$$\max W_{eff} = \frac{(b+\sigma a)^3}{27M^2b^2(b-\sigma a)}.$$

We are only interested in the $0 \leq a < b$. This is because if this condition is violated $W_{eff} < 0$ for all $r$ and $b > 0$ therefore a plunge orbit is inevitable. In order to understand how variations in the values of the constants affect $W_{eff}$ we note that:

$$\lim_{b\to\sigma a}(\max W_{eff}) = \infty \quad \text{and} \quad \lim_{b\to-\sigma a}(\max W_{eff}) = 0$$

$$\lim_{b\to\sigma a}(r_c) = 0 \quad \text{and} \quad \lim_{b\to-\sigma a}(r_c) = \infty.$$

We still have:

$$\lim_{r\to\infty}(W_{eff}) = 0 \quad \text{and} \quad \lim_{r\to0}(W_{eff}) = -\infty.$$

So plotting $W_{eff}$ against $r$ and $\sigma a/b$ we get the plot in Figure 15. In this figure the cross-section taken at the required value of $\sigma a/b$ gives you the analog of the $W_{eff}$ graphs given in Section 4.5. Again we have scaled the axis by powers of $M$ to remove the $M$ dependence.

It is worth noting the following properties of the graph in Figure 15;

[33] A Mathematica notebook that does this can be found in Appendix C this was adapted from Appendix B which was adapted from a notebook provided on Hartle's website [16].

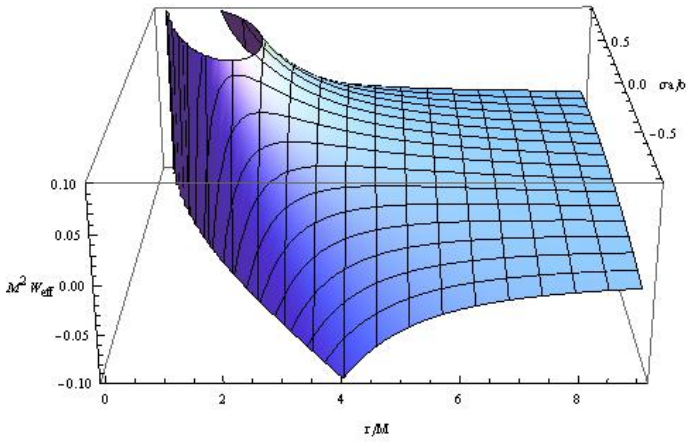


Figure 15: This plot indicates how $W_{eff}$ varies with $r$, $a$, $b$ and $\sigma$.The cross-section taken at the required value of $\sigma a/b$ gives you the analog of the $W_{eff}$ graphs given in Section 4.5. Notice how the peak value of $W_{eff}$ increases, and occurs at a smaller value of $r$, for greater values of $\sigma a/b$

- For any cross-section (ie any specific values of $b, a, \sigma$) there is only a single local maxima and no local minima. This means that the qualitative classification system, of plunge scatter and circular orbits, we used in the Schwarzschild case still applies.
- The shape of the $W_{eff}$ graph now depends on $b$ which was not true in the Schwarzschild case. This means that care needs to be taken when interpreting $W_{eff}$ as the effective potential. Equation (72) shows that this does not affect our ability to determine turning points in $r$ however it could in principle mean that even though the only turning point in $W_{eff}$ is maximal, circular orbits are still stable. In reality this is not the case and circular orbits are unstable however showing this would require a digression that is beyond our scope[34].
- The more the black hole is rotating with the light ray the smaller the radius of circular orbits. Furthermore the terning point in $r$ of scatter orbits is allowed to be smaller. This begs questions about the event horizon that will be discussed in Section 6.5.3. For retrograde orbits the result is the reverse.

[34]For how this may be done see Hobson et al. [3] - Section 13.18.

### 6.5.1 Circular Orbits

In order to have a circular orbit, as in the Schwarzschild case, we need:

$$\max W_{eff} = \frac{1}{b^2}.$$

This gives us the equation:

$$(b + \sigma a)^3 = 27M^2 (b - \sigma a)$$

Substituting $b + \sigma a = v + 9M^2/v$ into the above and rearranging we get[35]:

$$\left(v + \frac{9M^2}{v}\right)^3 = 27M^2 \left(v + \frac{9M^2}{v} - 2\sigma a\right)$$

$$\Rightarrow v^3 + 3 \times 9M^2 v + \frac{3 \times 9^2 M^4}{v} + \frac{9^3 M^6}{v^3} = 27M^2 v + \frac{27 \times 9M^4}{v} - 2 \times 27M^2 \sigma a$$

$$\Rightarrow v^6 + 54M^2 \sigma a v^3 + 9^3 M^6 = 0.$$

Using the quadratic equation we the find that:

$$v = 3M \left(\frac{-\sigma a}{M} \pm i\sqrt{1 - \left(\frac{a}{M}\right)^2}\right)^{1/3}.$$

We can now undo our substitution and we get:

$$b = 3M \left(-\frac{\sigma a}{M} \pm i\sqrt{1 - \left(\frac{a}{M}\right)^2}\right)^{1/3} + \frac{3M}{\left(-\frac{\sigma a}{M} \pm i\sqrt{1 - \left(\frac{a}{M}\right)^2}\right)^{1/3}} - \sigma a$$

Multiplying top and bottom by the complex conjugate of the denominator of the second term gives:

$$b = 3M \left(-\frac{\sigma a}{M} \mp i\sqrt{1 - \left(\frac{a}{M}\right)^2}\right)^{1/3} \left(\left(-\frac{\sigma a}{M} \pm i\sqrt{1 - \left(\frac{a}{M}\right)^2}\right)^{2/3} + 1\right) - \sigma a$$

This simplifies too:

$$b = 3M \left(\left(-\frac{\sigma a}{M} \pm i\sqrt{1 - \left(\frac{a}{M}\right)^2}\right)^{1/3} + \left(-\frac{\sigma a}{M} \mp i\sqrt{1 - \left(\frac{a}{M}\right)^2}\right)^{1/3}\right) - \sigma a$$

$$\Rightarrow b = 3M \left(\left(e^{i \arccos \frac{-\sigma a}{M}}\right)^{1/3} + \left(e^{-i \arccos \frac{-\sigma a}{M}}\right)^{1/3}\right) - \sigma a$$

[35] For the source of this substitution see Weisstein [21].

$$\Rightarrow b = 6M\cos\left(\frac{1}{3}\arccos\frac{-\sigma a}{M}\right) - \sigma a.$$

We can now use the half angle formula to get:

$$b = 6M\left(\frac{1}{2}\left[1+\cos\left(\frac{2}{3}\arccos\left[-\frac{\sigma a}{M}\right]\right)\right]\right)^{1/2} - \sigma a.$$

Thus circular orbits occur when:

$$b = 3\left(2M^2\left[1+\cos\left(\frac{2}{3}\arccos\left[-\frac{\sigma a}{M}\right]\right)\right]\right)^{1/2} - \sigma a \tag{74}$$

and have a radius of:

$$r_c = 2M\left[1+\cos\left(\frac{2}{3}\arccos\left[-\frac{\sigma a}{M}\right]\right)\right]. \tag{75}$$

Giving:

$$b = 3\sqrt{Mr_c} - \sigma a. \tag{76}$$

Note that for a Kerr black hole of given angular momentum ($J$) and mass ($M$) in general there will be 2 possible circular orbits, one prograde and one retrograde. For this reason we, henceforth, denote radii of these orbits $r_{c+}$ (prograde) and $r_{c-}$ (retrograde) and their corresponding impact parameters, $b_{c+}$ and $b_{c-}$. Thus we have:

$$r_{c\pm} = 2M\left[1+\cos\left(\frac{2}{3}\arccos\left[\mp\frac{a}{M}\right]\right)\right]$$

and:

$$b_{c\pm} = 3\sqrt{Mr_{c\pm}} \mp \sigma a.$$

Do not be misled by the signs attributed to the radii as these correspond to the value of $\sigma$ and not their magnitude. Figure 15 indicates that:

$$r_{c+} \leq r_{c-} \quad \text{and} \quad b_{c+} \leq b_{c-}.$$

It is also clear from this figure that these two orbits only coincide when $a = 0$, i.e. the Schwarzschild case, and move progressively further apart for larger $a$.

In the graphs that make up Figure 16 we show these two circular orbits for $a = 0.5$. The green graphs are for $\sigma = 1$. The blue graphs are for $\sigma = -1$. The direction of rotation of the black hole is indicated in yellow and the values of $1/b_{c\pm}^2$ in red. Care must be taken in interpreting the coordinates $(x, y)$ in the trajectory graphs for reasons discussed in Section 6.2.

Figure 16: In this figure we see the two possible circular orbits of a Kerr black hole with $a = 0.5$. The left graph shows the values of $b$ required for these orbits, and why these orbits are circular.

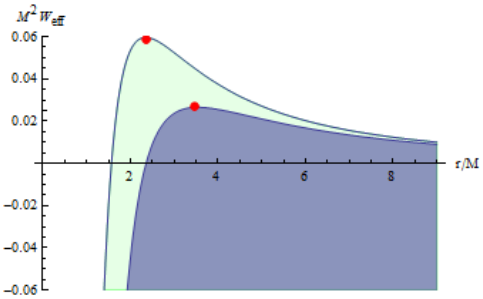


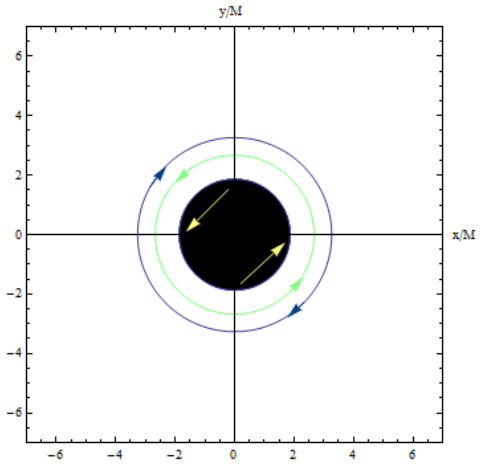


### 6.5.2 Prograde vs. Retrograde

In the graphs of Figures 17, 18 and 19 corotating orbits are shown in green and counterrotating in blue. As ever the value $1/b^2$ is in red. To highlight the difference sigma makes the orbits are shown to be coming from the same place, though in fact they are coming from opposite sides. The qualitative shape of each trajectory still relies only on the relationship between $b$ and $\max W_{eff}$ so it would be superfluous to analyze the turning points of each graph individually, as this has been done in Section 4.5, and the result is very similar.

Figure 17: Both the prograde (green) and retrograde (blue) photons follow plunge orbits. The images are shown superimposed on each other, though one of them has been reflected about the $y/M$ axis.

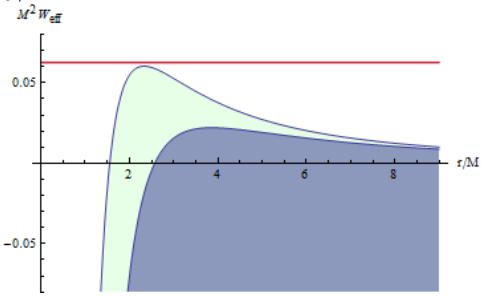


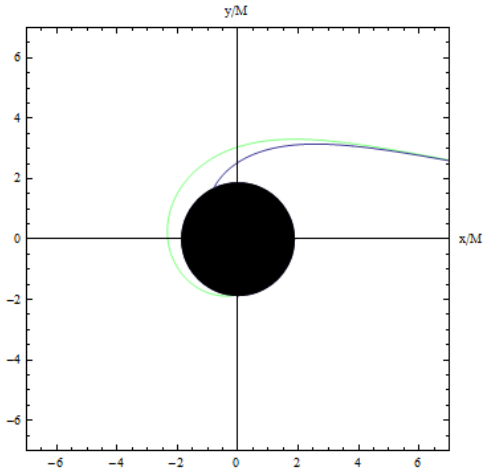

Figure 18: Both the prograde (green) and retrograde (blue) photons follow scatter orbits. The images are shown superimposed on each other, as before.

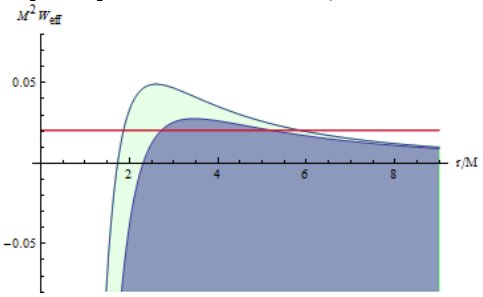


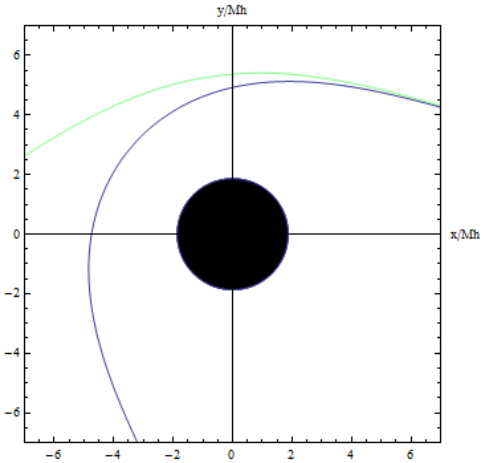


Figure 19: In this Figure the prograde (green) photons follow a scatter orbit and the retrograde (blue) photons a plunge orbit. Again the images are shown superimposed on each other.

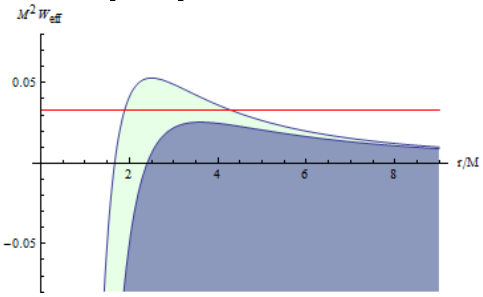


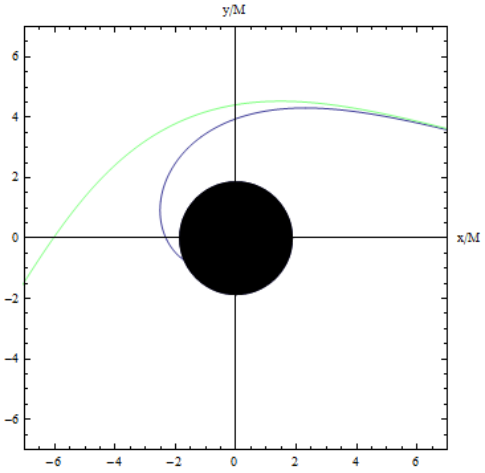


The other factors that affect the trajectory are $b$ and $a$. The discussion of variation in $b$ is essentially the same as in the Schwarzschild case so a further discussion is unnecessary. That leaves a discussion of the effect of $a$ which will take place in the next section.

### 6.5.3 Variation in Angular Momentum per Unit Mass

Figure 15 shows that, for $\sigma = 1$, as $a$ increases the radius of circular orbits decreases. Correspondingly the minimum value of $r$ ($r_0$) attainable by scattering orbits decreases. Clearly this can not go on indefinitely as otherwise it would allow scatter orbit to pass within the outer event horizon which produces a contradiction. If we take the positive part of equation (66), i.e. the equation for the union of outer event horizon and the equatorial plane, we have:

$$r_+ = M + \sqrt{M^2 - a^2}.$$

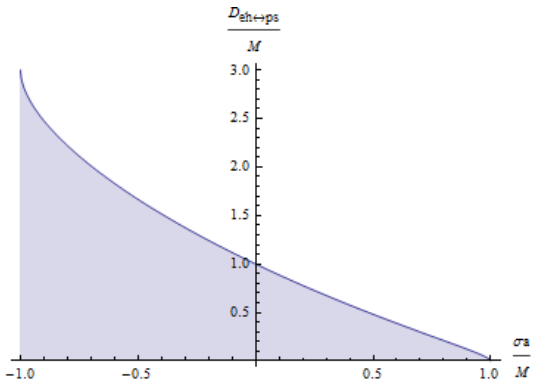


Figure 20:

We also have that:

$$\lim_{b\to{}^{+}b_{c+}} r_0 = r_{c+} = 2M\left[1+\cos\left(\frac{2}{3}\arccos\left[-\frac{a}{M}\right]\right)\right]$$

since the closest a scatter orbit can get to a black hole is to just miss the inner photon sphere[36]. The distance from the outer event horizon to the photon sphere ($D_{eh\leftrightarrow ps}$) is given by:

$$D_{eh\leftrightarrow ps} = r_{c+} - r_{+} = 2M\left[1+\cos\left(\frac{2}{3}\arccos\left[-\frac{a}{M}\right]\right)\right] - M - \sqrt{M^2-a^2}.$$

$$\Rightarrow \frac{r_{c+}-r_{+}}{M} = 1+2\cos\left(\frac{2}{3}\arccos\left[-\frac{a}{M}\right]\right) - \sqrt{1-\left(\frac{a}{M}\right)^2}.$$

It is not immediately obvious that this is greater than 0. However plotting $D_{eh\leftrightarrow ps}/M$ against $\sigma a/M$ we get Figure 20. This shows that for non naked singularities, i.e. $a^2 < M^2$, this distance is always greater than 0. It further shows that as $a \to M$ the radial distance between the photon sphere and the outer event horizon tends to 0. This means that prograde scatter orbits can get closer to Kerr black holes the faster they are rotating.

[36] Or it can become part of the photon sphere for a time before scattering due to instability.

# 7 Conclusion

It is not possible for us to perform a completely precise analysis of light-ray trajectories. However we can use numerical methods to give us an arbitrarily accurate approximation of a given system[37]. The appendices that follow provide Mathematica notebooks that do this. Despite this restriction, as this report has sought to demonstrate mathematically, we can use analytic techniques to determine the qualitative properties of the trajectories.

Light trajectories that start from $r = \infty$, lie in the equatorial plane of the black hole[38], and are solely influenced by an isolated black hole, which we place, without loss of generality, at the origin, fall into three qualitatively distinct categories. These are plunge, scatter and unstable circular orbits. For a black hole of given mass ($M$), and angular momentum per unit mass ($a$), the category into which the orbit falls is determined solely by the impact parameter $b$ and whether the orbit is retrograde or prograde ($\sigma$) via the following relations.

$$b = 3\left(2M^2\left[1+\cos\left(\frac{2}{3}\arccos\left[-\frac{\sigma a}{M}\right]\right)\right]\right)^{1/2} - \sigma a \Rightarrow \text{Circular orbit}$$

$$b > 3\left(2M^2\left[1+\cos\left(\frac{2}{3}\arccos\left[-\frac{\sigma a}{M}\right]\right)\right]\right)^{1/2} - \sigma a \Rightarrow \text{Scatter orbit}$$

$$b < 3\left(2M^2\left[1+\cos\left(\frac{2}{3}\arccos\left[-\frac{\sigma a}{M}\right]\right)\right]\right)^{1/2} - \sigma a \Rightarrow \text{Plunge orbit.}$$

We can use our understanding of scatter orbits to analyze gravitational lensing. By making a few approximations we can use this effect to come up with equations that help us calculate properties of the system. Most notably by using equation (62) to work out the Mass of the source of curvature. This is an important tool in astronomy and we have shown how it is derived from General Relativity theory.

[37] This isn't strictly speaking true in that there is a fundamental limit on the number of computations it is possible to make in any given period of time with a given computer. Using the algorithm of maximum efficiency this limits the accuracy that is achievable in a period of time. If the universe is closed then this means there is a fundamental limit on the accuracy of numerical calculations that may be achieved during the life of the universe. If the universe is open then the heat death predicted by the second law of thermodynamics would put an end to the possibility to further calculations. However it seems safe to assume that in any practical situation other constraints would apply first.

[38] All orbits of Schwarzschild black holes are equatorial

# Appendix A

## Geodesic Equation Solver

In[1]:=
```
Clear[coord, metric, inversemetric, affine, r, θ, ϕ, t]
```

In[2]:=
```
n = 4
```

Out[2]= 4

In[3]:=
```
coord = {t, r, θ, ϕ}
```

Out[3]= $\{t, r, \theta, \phi\}$

In[4]:=
```
metric =
 {{-(1 - 2 M/r), 0, 0, 0}, {0, (1 - 2 M/r)^-1, 0, 0}, {0, 0, r^2, 0}, {0, 0, 0, r^2 Sin[θ]}}
```

Out[4]=
$$\begin{pmatrix} \frac{2M}{r}-1 & 0 & 0 & 0 \\ 0 & \frac{1}{1-\frac{2M}{r}} & 0 & 0 \\ 0 & 0 & r^2 & 0 \\ 0 & 0 & 0 & r^2\sin(\theta) \end{pmatrix}$$

In[5]:=
```
inversemetric = Simplify[Inverse[metric]]
```

Out[5]=
$$\begin{pmatrix} \frac{r}{2M-r} & 0 & 0 & 0 \\ 0 & 1-\frac{2M}{r} & 0 & 0 \\ 0 & 0 & \frac{1}{r^2} & 0 \\ 0 & 0 & 0 & \frac{\csc(\theta)}{r^2} \end{pmatrix}$$

In[6]:=
```
affine := affine = Simplify[
   Table[1 / 2 Sum[(inversemetric[[i, s]]) * (D[metric[[s, j]], coord[[k]]] +
         D[metric[[s, k]], coord[[j]]] - D[metric[[j, k]], coord[[s]]]),
      {s, 1, n}], {i, 1, n}, {j, 1, n}, {k, 1, n}]]
```

In[7]:=
```
listaffine := Table[If[UnsameQ[affine[[i, j, k]], 0],
   {ToString[Γ[i, j, k]], affine[[i, j, k]]}], {i, 1, n}, {j, 1, n}, {k, 1, j}]
```

In[8]:=
```
TableForm[Partition[DeleteCases[Flatten[listaffine], Null], 2],
 TableSpacing → {2, 2}]
```

Out[8]//TableForm=

| | |
|---|---|
| Γ[1, 2, 1] | $-\frac{M}{2Mr-r^2}$ |
| Γ[2, 1, 1] | $\frac{M(r-2M)}{r^3}$ |
| Γ[2, 2, 2] | $\frac{M}{2Mr-r^2}$ |
| Γ[2, 3, 3] | $2M-r$ |
| Γ[2, 4, 4] | $\sin(\theta)(2M-r)$ |
| Γ[3, 3, 2] | $\frac{1}{r}$ |
| Γ[3, 4, 4] | $-\frac{\cos(\theta)}{2}$ |
| Γ[4, 4, 2] | $\frac{1}{r}$ |
| Γ[4, 4, 3] | $\frac{\cot(\theta)}{2}$ |

In[9]:=
```
geodesic := geodesic = Simplify[Table[-Sum[affine[[i, j, k]] u[j] u[k], {j, 1, n},
      {k, 1, n}], {i, 1, n}]]
```

In[10]:=
```
listgeodesic := Table[{"d/dλ" ToString[u[i]], "=", geodesic[[i]]}, {i, 1, n}]
```

In[11]:=
```
TableForm[listgeodesic, TableSpacing → {2}]
```

Out[11]//TableForm=

| | | |
|---|---|---|
| d/dλ u[1] | = | $\frac{2Mu(1)u(2)}{2Mr-r^2}$ |
| d/dλ u[2] | = | $\frac{Mu(1)^2(2M-r)}{r^3}-\frac{Mu(2)^2}{2Mr-r^2}-u(4)^2\sin(\theta)(2M-r)-u(3)^2(2M-r)$ |
| d/dλ u[3] | = | $\frac{1}{2}u(4)^2\cos(\theta)-\frac{2u(2)u(3)}{r}$ |
| d/dλ u[4] | = | $-\frac{u(4)(ru(3)\cot(\theta)+2u(2))}{r}$ |

In[12]:=
```
Clear[listgeodesic]
```

In[13]:=
```
listgeodesic := Table[{"d/dλ" ToString[u[i]], "=", geodesic[[i]]}, {i, 1, n}]
```

In[14]:=
```
TableForm[listgeodesic, TableSpacing → {2}]
```

Out[14]//TableForm=

| | | |
|---|---|---|
| d/dλ u[1] | = | $\frac{2Mu(1)u(2)}{2Mr-r^2}$ |
| d/dλ u[2] | = | $\frac{Mu(1)^2(2M-r)}{r^3}-\frac{Mu(2)^2}{2Mr-r^2}-u(4)^2\sin(\theta)(2M-r)-u(3)^2(2M-r)$ |
| d/dλ u[3] | = | $\frac{1}{2}u(4)^2\cos(\theta)-\frac{2u(2)u(3)}{r}$ |
| d/dλ u[4] | = | $-\frac{u(4)(ru(3)\cot(\theta)+2u(2))}{r}$ |

This notebook is an adaptation of one provided by Hartle [16], in the Mathematica Notebooks Section, entiteled Christoffel.

# Appendix B

## Light Orbits in Schwarzschild Geometry

The only parameter that needs to be entered is **b**; for plunge orbits enter **b<**$\sqrt{27}$ , for scatter orbits enter **b>**$\sqrt{27}$ and for circular orbits enter **b=**$\sqrt{27}$ .

In[1]:=
```
Clear["Global`*"]
```

In[2]:=
```
b = 5
```

Out[2]= 5

In[3]:=
```
V[u_] := u^2 - 2 u^3
```

In[4]:=
```
Weff = Plot[V[1 / r], {r, 0, 9}, PlotRange → 0.05,
  AxesLabel -> {"r/M", "M^2W_eff"}, AxesOrigin → {0, 0}, Filling → Bottom]
```

Out[4]=

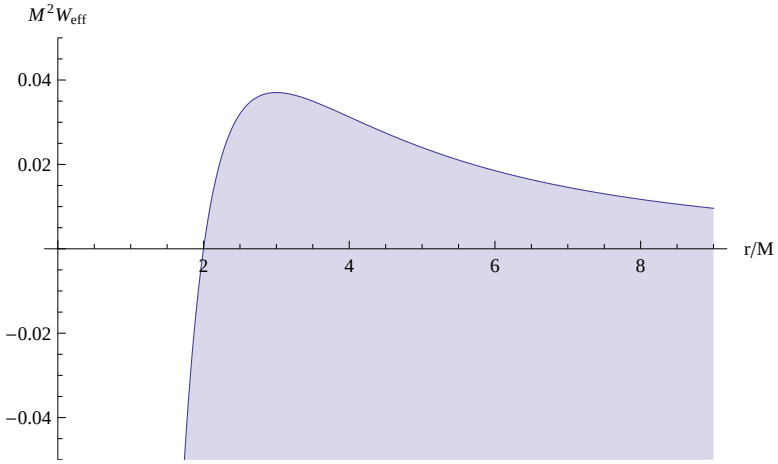


In[5]:=
```
dV := D[V[u], u]
```

In[6]:=
```
max = 1 / 3
```

Out[6]= $\frac{1}{3}$

In[7]:=
```
wmax = V[1 / 3]
```

Out[7]= $\frac{1}{27}$

In[8]:=
```
sce := Plot[1 / b^2, {r, 0, 9}, DisplayFunction → Identity]
```

In[9]:=
```
Show[Weff, sce, DisplayFunction → $DisplayFunction]
```

Out[9]=

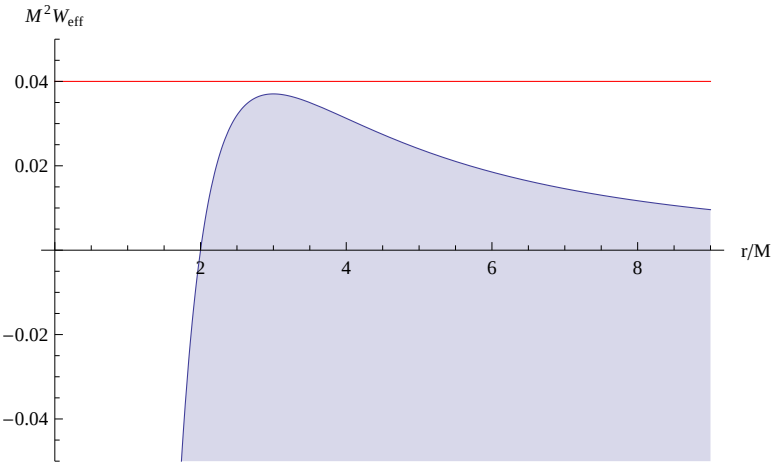


In[11]:=
```
soln = NSolve[V[tp] == 1 / b^2, tp]
```

Out[11]= $\{\{\text{tp} \to -0.172458\}, \{\text{tp} \to 0.336229 - 0.0540431\, i\}, \{\text{tp} \to 0.336229 + 0.0540431\, i\}\}$

In[12]:=
```
tp1 = tp /. soln[[1]]
```

Out[12]= $-0.172458$

In[13]:=
```
tp2 = tp /. soln[[2]]
```

Out[13]= $0.336229 - 0.0540431\, i$

In[14]:=
```
tp3 = tp /. soln[[3]]
```

Out[14]= $0.336229 + 0.0540431\, i$

In[15]:=
```
rst = 20
```

Out[15]= 20

In[16]:=
```
ust = 1 / rst
```

Out[16]= $\frac{1}{20}$

In[17]:=
```
eps = 0.00000001
```

Out[17]= $1. \times 10^{-8}$

In[18]:=
```
orbittype :=
 If[(1 / b^2) == wmax, "circle", If[(1 / b^2) < wmax, "scatter", "plunge"]]
```

In[19]:=
```
orbittype
```

Out[19]= plunge

In[20]:=
```
norbit := If[orbittype == "plunge", 0.5, If[orbittype == "circle", 2 π, 1]]
```

In[21]:=
```
u1 := If[orbittype == "circle", tp2 (1 + eps), ust]
```

In[22]:=
```
u2 := If[orbittype == "plunge", 0.5 (1 - eps), tp2 (1 - eps)]
```

In[23]:=
```
norbit
```

Out[23]= 0.5

In[24]:=
```
u1
```

Out[24]=
$$\frac{1}{20}$$

In[25]:=
```
u2
```

Out[25]=
$$0.5$$

In[26]:=
```
theta[u_, b_, u1_] := NIntegrate[(1 / b^2 - V[w])^(-1 / 2), {w, u1, u}]
```

In[27]:=
```
delphi = If[orbittype == "circle", 0, theta[u2, b, u1]]
```

Out[27]=
$$4.37462$$

In[28]:=
```
n[z_] := IntegerPart[z]
```

In[29]:=
```
zf[z_] := FractionalPart[z]
```

In[30]:=
```
ua[z_] := u1 (1 - 2 zf[z]) + u2  2 zf[z]
```

In[31]:=
```
ub[z_] := u1 (2 zf[z] - 1) + 2 u2 (1 - zf[z])
```

In[32]:=
```
u[z_] := If[zf[z] < .5, ua[z], ub[z]]
```

In[33]:=
```
phia[z_] := 2 (n [z]) delphi + theta[u[z], b, u1]
```

In[34]:=
```
phib[z_] := 2 (n [z] + 1) delphi - theta[u[z], b, u1]
```

In[35]:=
```
accphi[z_] := If[orbittype == "circle", z, If[zf[z] < .5, phia[z], phib[z]]]
```

In[36]:=
```
x[z_] := Cos[accphi[z]] / u[z]
```

In[37]:=
```
y[z_] := Sin[accphi[z]] / u[z]
```

In[38]:=
```
graph = ParametricPlot[{x[t], y[t]}, {t, 0, norbit},
  Method -> {MaxBend -> .001, PlotDivision → 500},
  AspectRatio → Automatic, PlotRange → 5, AxesLabel -> {"x/M", "y/M"}]
```

Out[38]=

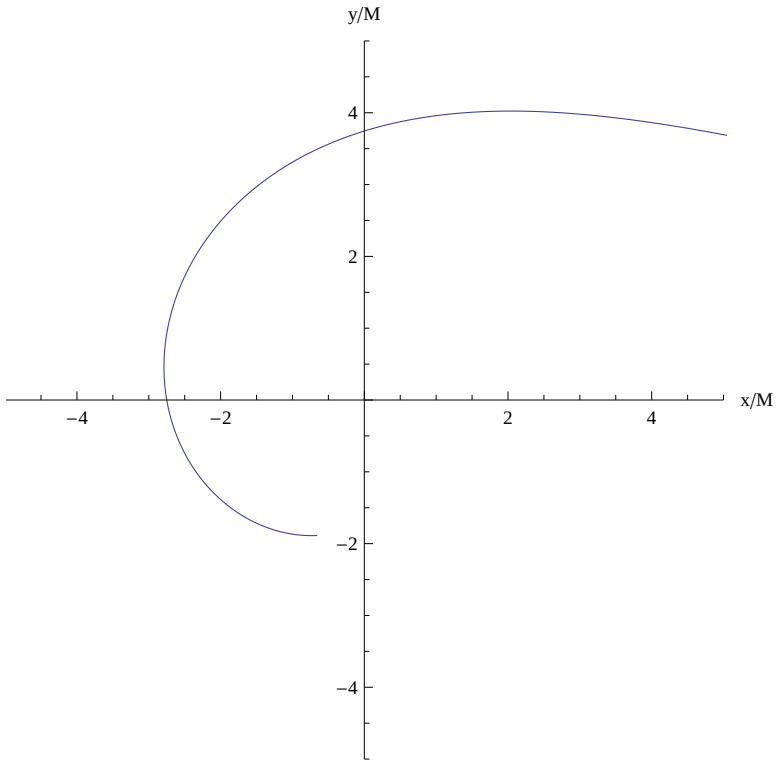

In[39]:=
```
eh = ParametricPlot[{r Sin[k], r Cos[k]}, {k, 0, 2 π},
  {r, 0, 2}, PlotRange → 5, AxesLabel -> {"x/M", "y/M"}, Mesh → False]
```

Out[39]=

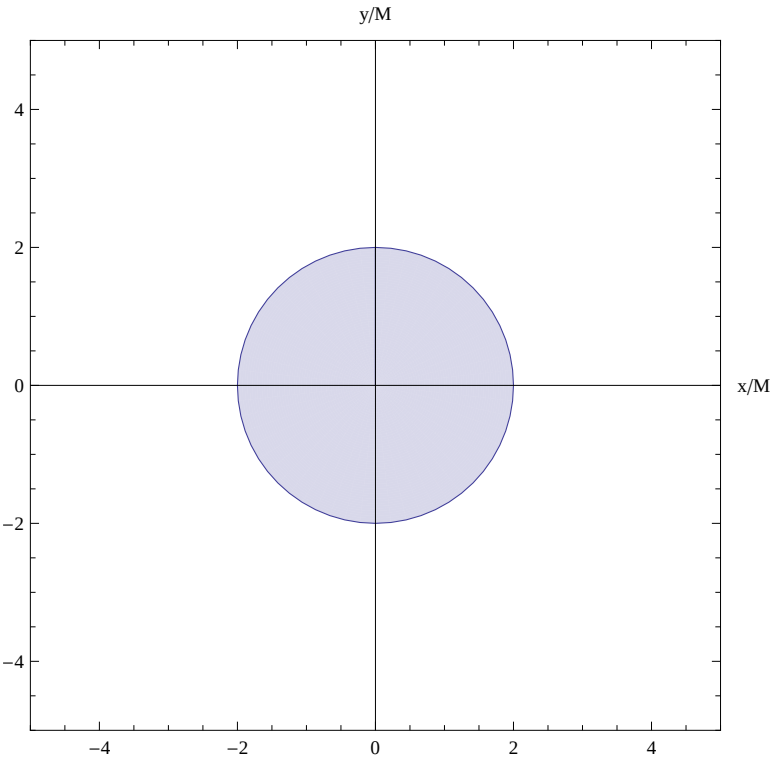


In[40]:=
```
Show[eh, graph, DisplayFunction → $DisplayFunction]
```

Out[40]=

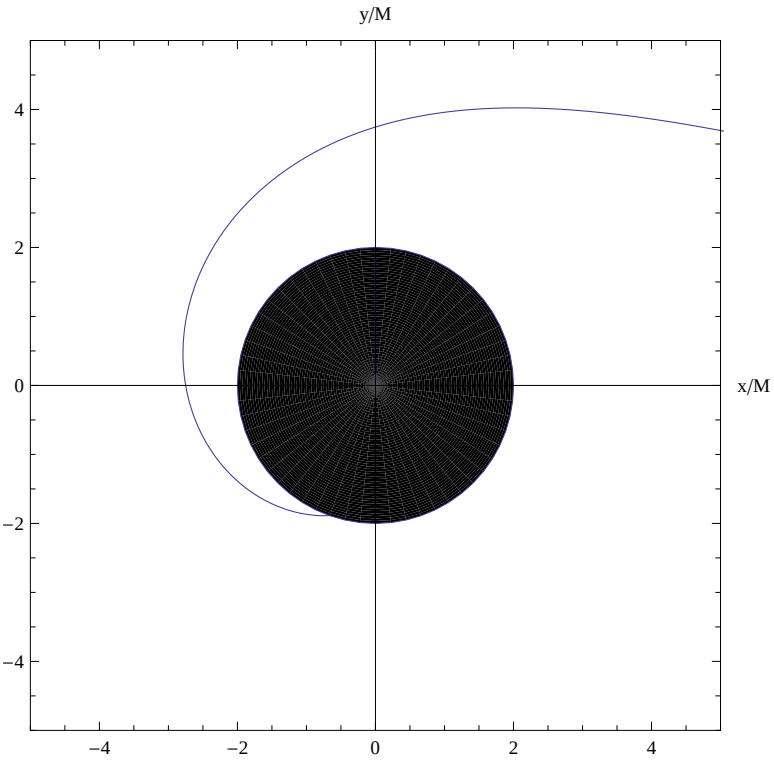


This notebook is an adaptation of one provided on Hartle's website [16], in the Mathematica Notebooks Section, entiteled Schwarzorbits.

# Appendix C

## Light Trajectories In Kerr Geometry

Three parameters need to be entered; $\sigma$, **a** and **b**. $\sigma$ needs to be chosen as +1 for prograde or -1 for retrograde orbits, **a** should be chosen such that **a<1**. b should be chosen suchg that **b>a**. For circular motion enter **b=Bc**, for scatter orbits enter **b>Bc** and for plunge orbits enter **b<Bc**.

In[1]:=
```
Clear["Global`*"]
```

In[2]:=
```
a = 0.9
```

Out[2]= 0.9

In[3]:=
```
σ = 1
```

Out[3]= 1

In[4]:=
```
co[B_] = (1 - (a / B)^2)^3 / (27 (1 - σ (a / B))^4) - 1 / B^2
```

Out[4]= $\frac{\left(1-\frac{0.81}{B^2}\right)^3}{27\left(1-\frac{0.9}{B}\right)^4}-\frac{1}{B^2}$

In[5]:=
```
CO = Solve[co[B] == 0, B, Reals]
```

Out[5]= $\{\{B\to -6.83232\},\{B\to 0.9\},\{B\to 0.9\},\{B\to 0.9\},\{B\to 1.2879\},\{B\to 2.84442\}\}$

In[6]:=
```
B /. %
```

Out[6]= $\{-6.83232, 0.9, 0.9, 0.9, 1.2879, 2.84442\}$

In[7]:=
```
Bc = Max[%]
```

Out[7]= 2.84442

In[8]:=
```
b = 3.5
```

Out[8]= 3.5

In[9]:=
```
W[u_] := (1 - (a / b)^2) u^2 - 2 (1 - σ × (a / b))^2 u^3
```

In[10]:=
```
Weff = Plot[W[1 / r], {r, 0, 9}, PlotRange → 0.14,
  AxesLabel -> {"r/M", "M^2W_eff"}, AxesOrigin → {0, 0}, Filling → Bottom]
```

Out[10]=

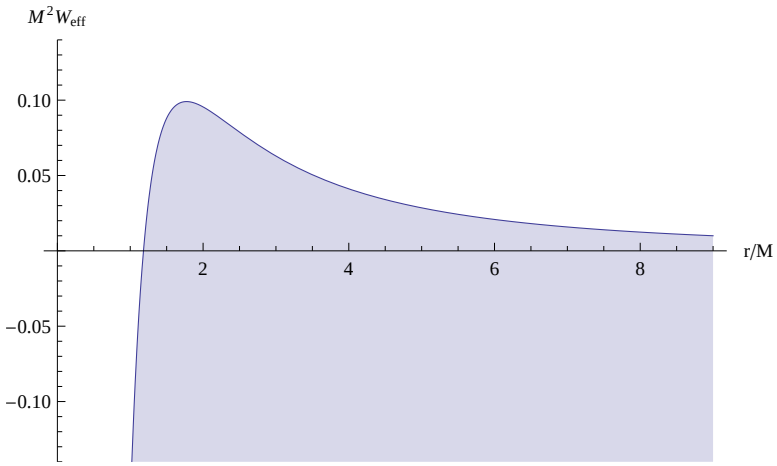


In[11]:=
```
dW[f_] := D[W[f], f]
```

In[12]:=
```
dW[f]
```

Out[12]= $1.86776\, f - 3.31102\, f^2$

In[13]:=
```
max = NSolve[dW[ex] == 0, ex]
```

Out[13]= {{ex → 0.}, {ex → 0.564103}}

In[14]:=
```
ufwm = ex /. max[[2]]
```

Out[14]= 0.564103

In[15]:=
```
Wmax = W[ufwm]
```

Out[15]= 0.0990569

In[16]:=
```
sce := Plot[1 / b^2, {r, 0, 9}, DisplayFunction → Identity]
```

In[17]:=
```
Show[Weff, sce, DisplayFunction → $DisplayFunction]
```

Out[17]=

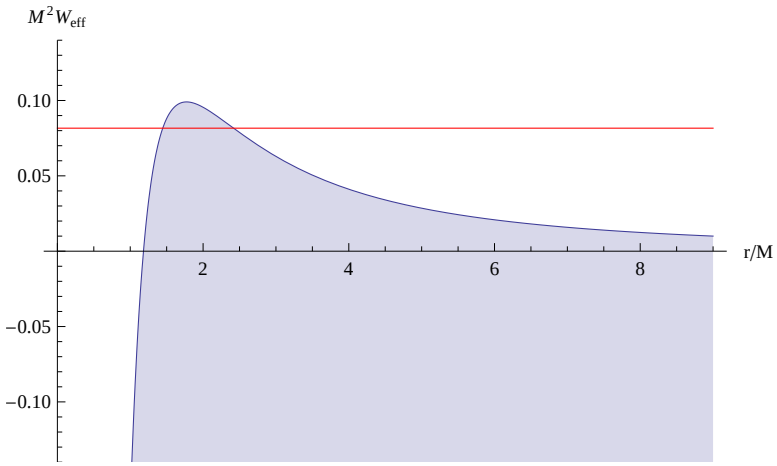


In[19]:=
```
soln = NSolve[W[tp] == 1 / b^2, tp]
```

Out[19]= {{tp → −0.258733}, {tp → 0.413438}, {tp → 0.69145}}

In[20]:=
```
tp1 = tp /. soln[[1]]
```

Out[20]= $-0.258733$

In[21]:=
```
tp2 = tp /. soln[[2]]
```

Out[21]= 0.413438

In[22]:=
```
tp3 = tp /. soln[[3]]
```

Out[22]= 0.69145

In[23]:=
```
rst = 20
```

Out[23]= 20

In[24]:=
```
ust = 1 / rst
```

Out[24]= $\frac{1}{20}$

In[25]:=
```
eps = 0.00000001
```

Out[25]= $1.\times 10^{-8}$

In[26]:=
```
orbittype :=
 If[(1 / b^2) == Wmax, "circle", If[(1 / b^2) < Wmax, "scatter", "plunge"]]
```

In[27]:=
```
orbittype
```

Out[27]= scatter

In[28]:=
```
norbit := If[orbittype == "plunge", 0.5, If[orbittype == "circle", 2 π, 1]]
```

In[29]:=
```
u1 := If[orbittype == "circle", tp2 (1 + eps), ust]
```

In[30]:=
```
u2 := If[orbittype == "plunge", (1 - eps) / (1 + (1 - a^2)^0.5), tp2 (1 - eps)]
```

In[31]:=
```
norbit
```

Out[31]= 1

In[32]:=
```
u1
```

Out[32]= $\frac{1}{20}$

In[33]:=
```
u2
```

Out[33]= 0.413438

In[34]:=
```
theta[u_, b_, u1_] := NIntegrate[(1 / b^2 - W[w])^(-1 / 2), {w, u1, u}]
```

In[35]:=
```
delphi = If[orbittype == "circle", 0, theta[u2, b, u1]]
```

Out[35]= 2.51897

In[36]:=
```
n[z_] := IntegerPart[z]
```

In[37]:=
```
zf[z_] := FractionalPart[z]
```

In[38]:=
```
ua[z_] := u1 (1 - 2 zf[z]) + u2  2 zf[z]
```

In[39]:=
```
ub[z_] :=  u1 (2 zf[z] - 1)  + 2 u2 (1 - zf[z])
```

In[40]:=
```
u[z_] := If[orbittype == "circle",
   (1 - (a / b)^2) / (3 (1 - σ (a / b))), If[zf[z] < .5, ua[z], ub[z]]]
```

In[41]:=
```
phia[z_] := 2 (n [z]) delphi + theta[u[z], b, u1]
```

In[42]:=
```
phib[z_] := 2 (n [z] + 1) delphi - theta[u[z], b, u1]
```

In[43]:=
```
accphi[z_] := If[orbittype == "circle", z, If[zf[z] < .5, phia[z], phib[z]]]
```

In[44]:=
```
x[z_] := Cos[accphi[z]] / u[z]
```

In[45]:=
```
y[z_] := Sin[accphi[z]] / u[z]
```

In[46]:=
```
graph = ParametricPlot[{x[t], y[t]}, {t, 0, norbit},
  Method -> {MaxBend -> .001, PlotDivision → 5000},
  AspectRatio → Automatic, PlotRange → 7, AxesLabel -> {"x/M", "y/M"}]
```

Out[46]=

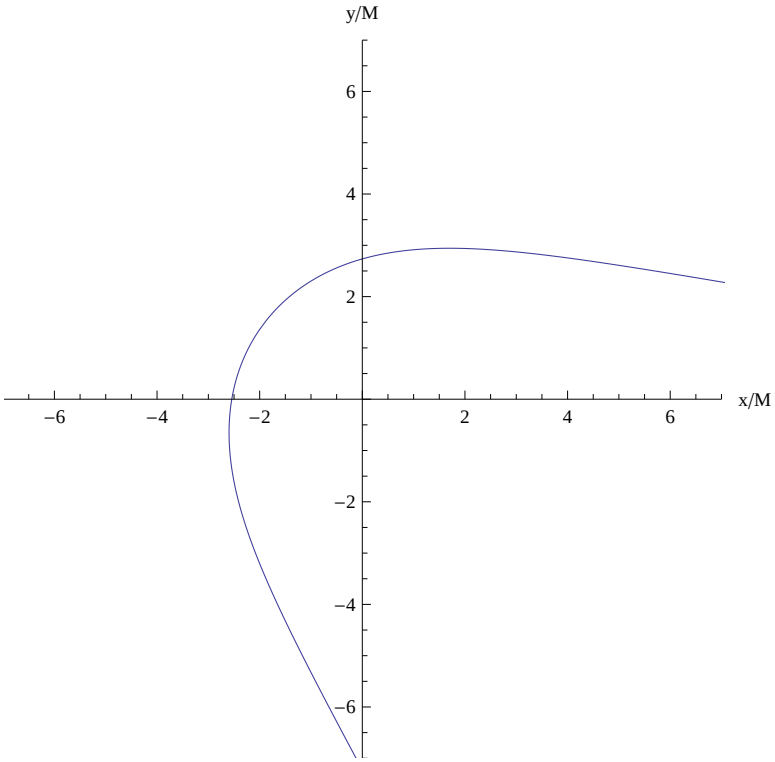


In[47]:=

In[48]:=
```
eh = ParametricPlot[{r Cos[t], r Sin[t]}, {t, 0, 2 π}, {r, 0, 1 + (1 - a^2)^0.5},
  PlotRange → 7, AxesLabel -> {"x/M", "y/M"}, Mesh → False]
```

Out[48]=

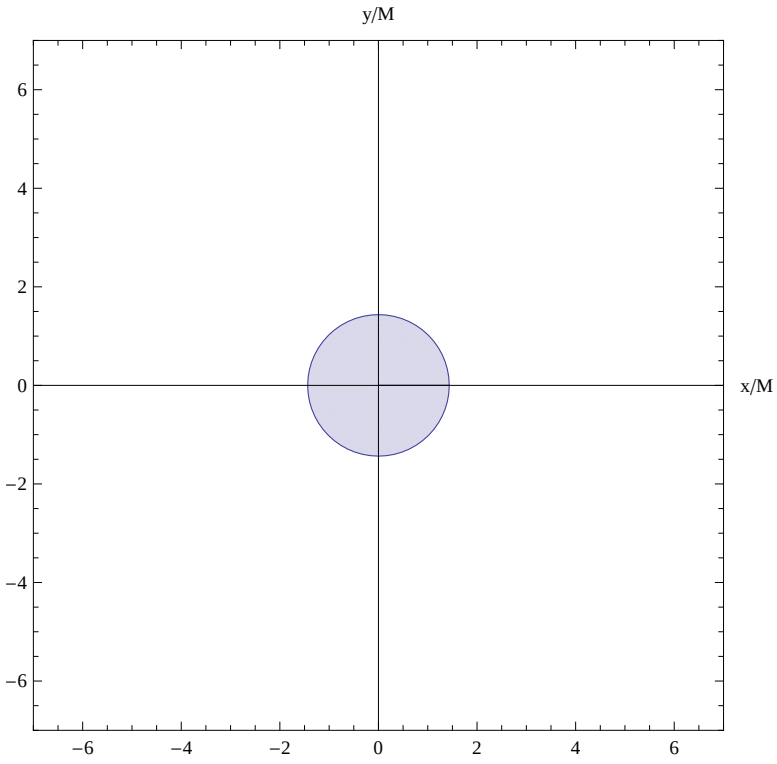


In[49]:=
```
Show[eh, graph, DisplayFunction → $DisplayFunction]
```

Out[49]=

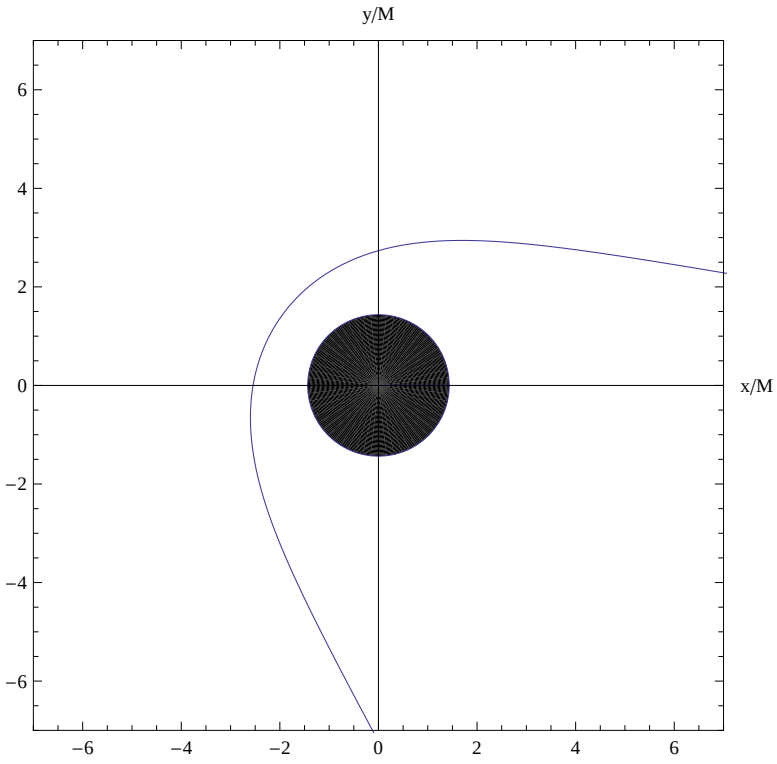


This notebook is an adaptation of one provided by Hartle [16], in the Mathematica Notebooks Section, entiteled Schwarzorbits.

# References


[1] James B Hartle, *Gravity an Introduction to Einstein's General Relativity*, Addison Wesley, San Francisco, 2003

[2] Tai L. Chow, *Gravity, Black Holes, and the Very Early Universe*, Springer Science+Business Media, New York, 233 Springer Street, 2008

[3] M. P. Hobson, G. Efstathiou, A. N. Lasenby, *General Relativity An Introduction for Physicists*, Cambridge University Press, The Edinburgh Building, CB2 2RU, 2006

[4] Robert M. Wald, *General Relativity*, University of Chicago Press, London, 1984

[5] Nathan Cohen, *Gravity's Lens*, John Wiley and Sons, Chichester, 1988

[6] Barrett O'Neill, *The Geometry of Kerr Black Holes*, A K Peters, Wellesley, Massachusetts, 1995

[7] J. Ehlers and P. Schneider, *Gravitational Lensing*, Edited By R J Gleiser, C N Kozameh, O M Moreschi, *General Relativity and Gravitation: Proceedings of the 13th International Conference on General Relativity and Gravitation*, Institute of Physics Publishing, Techno House, Redcliffe Way, Bristol, BS1 6NX, 1992

[8] Warren, S. J., Hewett, P. C., Lewis, G. F., Moller, P., Iovino, A., and Shaver, *A candidate optical Einstein ring*, Monthly Notices of the Royal Astronomical Society, Volume 278, Issue 1, pp. 139-145, 1996

[9] R. H. Boyer and R. W. Lindquist, *Maximal Analytic Extension of the Kerr Metric*, Journal of Mathematical Physics, Volume 8, Number 2, pp. 265-282, 1976

[10] J. D. Bekenstein, *Black Holes and The Second Law*, Letere Al Nuovo Cimento, Volume 4, Number 15, pp. 737-740, 1972

[11] Robert J. Nemiroff, *Visual Distortions Near a Neutron Star and Black Hole*, American Journal of Physics, Volume 61, pp. 619-631, 1993

[12] Y. C. Leung C. G. Wang *Minimum Mass of a Neutron Star*, Nature Physical Science, Volume 240, pp. 132-133, 1972

[13] Eric W. Weisstein, *Schwarzschild, Karl (1873-1916)*, Wolfram Research, `http://scienceworld.wolfram.com/biography/Schwarzschild.html`, written: 1996, viewed: 2011

[14] Authorship unknown, *Roy P. Kerr.*, Encyclopaedia Britannica, `http://www.britannica.com/EBchecked/topic/315523/Roy-P-Kerr`, written: Unknown, viewed: 2011

[15] Sean M. Carroll, *Lecture Notes on General Relativity*, Enrico Fermi Institute University of Chicago, http://nedwww.ipac.caltech.edu/level5/March01/Carroll3/Carroll1.html, written: 1997, viewed: 2011

[16] James B. Hartle, *Gravity an Introduction to Einstein's General Relativity*, Addison Wesley, San Francisco, http://wps.aw.com/aw_hartle_gravity_1/7/2001/512494.cw/index.html, written: 2003, viewed: 2011

[17] J. J. O'Connor and E. F. Robertson, *Wilhelm Karl Joseph Killing*, School of Mathematics and Statistics - University of St Andrews, Scotland, http://www-history.mcs.st-and.ac.uk/Biographies/Killing.html, written: 2005, viewed: 2011

[18] Gene Smith, *Gravitational Lenses*, University of California, San Diego Center for Astrophysics & Space Sciences, http://casswww.ucsd.edu/public/tutorial/GLens.html, created: 1999, viewed: 2011

[19] Author Unknown, *Gravitational Lens001*, Washington University in St. Louis, http://www.epsc.wustl.edu/classwork/classwork_210a/transparencies/bernard/gravitational_lens001.jpgl, created: 2008, viewed: 2011

[20] Hubble Telescope, *Picture Album: Einstein Ring Gravitational Lens*, NASA, http://hubblesite.org/gallery/album/entire/pr2005032g/web/, taken: unclear, viewed: 2011

[21] Eric Weisstein, *Cubic Formula*, Wolfram MathWorld, http://mathworld.wolfram.com/CubicFormula.html, written: 1999, viewed: 2011

[22] Joachim Wambsganss, *Gravitational Lensing in Astronomy*, Astrophysikalisches Institut Potsdam, http://hermes.aei.mpg.de/lrr/1998/12/article.xhtml, written: 1998, viewed: 2011